Available online at www.sciencedirect.com

SCIENCE DIRECT®

Coastal Engineering 51 (2004) 991–1020

Coastal Engineering
An International Journal for Coastal, Harbour and Offshore Engineers

www.elsevier.com/locate/coastaleng

2-D numerical analysis of near-field flow at low-crested permeable breakwaters

N. Garcia*, J.L. Lara, I.J. Losada

Ocean and Coastal Research Group, University of Cantabria, Dpto. de Ciencias y Tecnicas del Agua y del Medio Ambiente, E.T.S.I. de Caminos, Canales y Puertos, Avda. de los Castros s/n, Santander 39005, Spain

Received 23 July 2003; received in revised form 1 July 2004; accepted 2 July 2004
Available online 16 September 2004

Abstract

This paper describes the capability of a numerical model named COrnell BReaking waves And Structures (COBRAS) [Lin, P., Liu, P.L.-F., 1998. A numerical study of breaking waves in the surf zone. Journal of Fluid Mechanics 359, 239–264; Liu, P.L.-F., Lin, P., Chang, K.A., Sakakiyama, T., 1999. Numerical modeling of wave interaction with porous structures. Journal of Waterway, Port, Coastal and Ocean Engineering 125, 322–330, Liu, P.L.-F., Lin, P., Hsu, T., Chang, K., Losada, I.J., Vidal, C., Sakakiyama, T., 2000. A Reynolds averaged Navier–Stokes equation model for nonlinear water wave and structure interactions. Proc. Coastal Structures '99, 169–174] based on the Reynolds Averaged Navier–Stokes (RANS) equations to simulate the most relevant hydrodynamic near-field processes that take place in the interaction between waves and low-crested breakwaters. The model considers wave reflection, transmission, overtopping and breaking due to transient nonlinear waves including turbulence in the fluid domain and in the permeable regions for any kind of geometry and number of layers. Small-scale laboratory tests were conducted in order to validate the model, with different wave conditions and breakwater configurations. In the present study, regular waves of different heights and periods impinging on a wide-crested structure are considered. Three different water depths were tested in order to examine the influence of the structure freeboard. The experimental set-up includes a flow recirculation system aimed at preventing water piling-up at the lee of the breakwater due to overtopping. The applicability and validity of the model are examined by comparing the results of the numerical computations with experimental data. The model is proved to simulate with a high degree of agreement all the studied magnitudes, free surface displacement, pressure inside the porous structure and velocity field. The results obtained show that this model represents a substantial improvement in the numerical modelling of low-crested structures (LCS) since it includes many processes neglected previously by existing models. The information provided by the model can be useful to analyse structure functionality, structure stability, scour and many other hydrodynamic processes of interest.

Keywords: Low-crested structures; RANS modelling; Flow in porous media; Wave transformation

* Corresponding author. Tel.: +34 942 201810; fax: +34 942 201860.
E-mail address: garciani@unican.es (N. Garcia).

0378-3839/$ - see front matter © 2004 Elsevier B.V. All rights reserved.
doi:10.1016/j.coastaleng.2004.07.017

1. Introduction

Low-crested structures (hereafter LCS) are increasingly regarded by coastal engineers and planners as a valuable alternative to more classical surface-piercing and/or hard structures. By low-crested structures we mean detached rubble-mound breakwaters built with the crown elevation near the still water level. Thus, these structures may be submerged, emerged, or both alternatively, but are characterized to be strongly overtopped. The increasing interest, for aesthetic, economical and environmental reasons, towards LCS makes a better understanding of their hydrodynamics crucial. These structures are primarily designed to reduce the wave loads on the coast through a series of wave transformation processes on and inside the structure that make the wave–structure interaction modelling very complex. The relative importance of each one of the physical processes, hereafter described, that take place in the interaction of a wave train with a low-crested structure depends on the wave parameters (height, period, relative depth) and on the rubble mound characteristics (geometry, porosity, permeability).

When the incident wave train impinges on the structure, part of the energy is reflected back to the sea and part is transmitted in the leeside zone. Reflection is an important characteristic of LCS as this type of structure is generally built with relatively steep slopes. The interferences between the incident and reflected waves give rise to standing wave patterns that affect the near-field flow and subsequently the stability of the structure. Besides, as waves shoal on the rising front of the structure, significant nonlinear effects occur, resulting in the amplification of bound waves (phase-locked with the primary wave). Most of the incident wave energy is lost on the structure's crest, essentially by breaking. Part of the energy is also dissipated by air entrainment and friction at the solid skeleton interface and within the porous media. For non-breaking waves, the flow resistance in the porous media is the main dissipation mechanism. Besides, during the breaking process, the bound waves enhanced at the shoaling stage of the propagation are released. Significant nonlinear interactions occur in the zone of the structure crest between the various wave phases and some energy is transferred from the fundamental wave frequency to higher harmonics (Driscoll et al., 1993; Beji and Battjes, 1994; Losada et al., 1996a,b). In the deeper waters of the leeside zone, the wave field is characterized by waves of complex form, with lower height and lower mean period. Due to the energy transfer from the fundamental harmonic to higher harmonic components, the incident narrow-banded spectrum turns into a broad-banded spectrum (Beji and Battjes, 1993). Besides, wave interaction with LCS gives rise to a series of three-dimensional phenomena, such as diffraction, 3D wave breaking and currents system generation, that will not be studied in the present paper exclusively dedicated to 2D processes.

An accurate description of all the mentioned wave transformation processes is needed to correctly assess the performance of the LCS. A series of studies have led through the years to a deeper knowledge of the low porous structures near-field and far-field influence, based on theoretical, experimental and numerical investigations. The complexity of the phenomena involved in the wave field interaction with LCS has led a great majority of investigators to resort to laboratory experiments, focusing especially on the prediction of wave transmission, reflection and energy dissipation. This is the case of works by Dick and Brebner (1968), Dattatri et al. (1978), Seelig (1980), Davies and Kriebel (1992), D'Angremond et al. (1996), Loveless and Debski (1997) or Seabrook and Hall (1998). Hattori and Sakai (1994) examined the conditions of incipient breaking over a permeable submerged structure. Loveless et al. (1998) focused on the phenomenon of sea level set-up behind detached breakwaters, previously investigated by Diskin et al. (1970), and pointed out the problem of water piling-up at the lee of low-crested structures in 2DV experiments.

Nonetheless, experimental investigation on low-crested structures has multifold problems: small-scale experiments are influenced by scale effects, large-scale models are expensive to build and measurements within breaking waves can be very complex, due to the aerated and transient nature of the water surface. As a consequence, alternative approaches, theoretical or numerical, have been considered for the study of wave–structure interaction. Theoretical approaches for sub-aerial breakwaters have been presented by Sollit and Cross (1972), Madsen and White (1976), Massel and Butowski (1980), Dalrymple et al. (1991), and

Losada et al. (1993). Wave transformation over submerged permeable breakwaters based on linear wave theory has been studied by Rojanakamthorn et al. (1989, 1990). Losada et al. (1996a,b) studied the hydrodynamics induced inside and outside a submerged permeable structure of rectangular or trapezoidal cross section under incoming regular wave trains, assuming potential flow and linear theory.

The progress in computation resources and the possibility of dealing with increasingly complex geometries has made the numerical approach more valuable. Kobayashi and Wurjanto (1989) developed a finite-difference model based on the shallow water equations for the study of monochromatic wave reflection, breaking and transmission over a submerged breakwater, but did not take into account the permeability of the breakwater. Wibbeler and Oumeraci (1992) presented a finite element model for the simulation of the wave-induced flow in a sub-aerial porous structure. Ohyama and Nadaoka (1992) modelled the transformation of nonlinear waves passing over a submerged impermeable breakwater using the boundary element method. Gu and Wang (1992) also used a boundary element method to model the interaction of monochromatic waves with breakwaters of irregular cross section, considering dissipation due to percolation and breaking effects. The model developed by Van Gent et al. (1994), based on the 2DV Navier–Stokes equations and the Volume Of Fluid (VOF) method introduced by Hirt and Nichols (1981), can simulate wave motions inside and outside permeable structures, including under breaking conditions, but does not take into account the turbulence generation–dissipation inside the porous media. Previous works on the same model were presented by Van der Meer et al. (1992) and Petit et al. (1994a,b). Other models based on Navier–Stokes equations using the SOLA-VOF method have been presented by Iwata et al. (1996) to investigate wave breaking features on a submerged impermeable structure and more recently by Troch and de Rouck (1998) for the simulation of wave interaction with a rubble-mound breakwater. Lin and Liu (1998) presented a VOF-type numerical model for studying the evolution of a wave train, shoaling and breaking in the surf zone, based on the Reynolds equations with a nonlinear k–ε model. Liu et al. (1999) included wave interaction with porous structures. Hsu et al. (2002) proposed a set of equations based on the Volume-Averaged/Reynolds Averaged Navier–Stokes (VARANS) equations to describe wave interaction with coastal structures. Volume-averaging allows the description of small-scale turbulence effects in the porous media. Hur and Mizutani (2003) investigated numerically the wave forces acting on a two-dimensional body installed on a submerged porous breakwater, combining the VOF and porous body models. Three-dimensional results are also presented. However, computational efforts for three-dimensional models based on RANS equations as well as Large Eddy Simulation (LES) approximations are still very time consuming nowadays. To date, the models based on two-dimensional RANS approximation are possibly the most adapted to the study of wave–structure interaction for engineering purposes, as computational efforts are reasonable and the number of simplifying assumptions is considerably reduced compared to other existing models.

As a conclusion of this review, a great number of investigations have been carried out in order to characterize the performance of low-crested structures, but few of these works considered the whole set of hydrodynamic processes associated with this type of structures. The numerical approach, with a model able to simulate wave breaking processes and porous flow effects, seems the most adequate for the study of nonbreaking and breaking wave interaction with low-crested structures. The model used in the present paper is the COrnell BReaking waves And Structures (COBRAS) model, initially developed by Lin (1998). This model has been used in previous works by Lin and Liu (1998) and Lara (2002), Lara et al. (submitted for publication) for the modelling of wave breaking over impermeable and permeable beds, or, as mentioned earlier, by Liu et al. (1999, 2000) and Hsu et al. (2002) for wave interaction with porous structures. The model considers wave reflection, transmission, overtopping and breaking due to transient nonlinear waves including turbulence in the fluid domain and in the permeable regions for any kind of geometry and number of layers.

The aim of this paper is to demonstrate the ability of the model to reproduce the hydrodynamics of low-crested structures and to investigate the main features of wave interaction with this type of structure. The

validation of the information provided by the model will allow further investigation of wave interaction with LCS essentially based on numerical data. The performance of the numerical model is verified through comparisons with experimental results from small-scale tests conducted at the University of Cantabria within the framework of the European Union project Design of Environmental LOw-crested coastal defence Structures (DELOS). The set-up of the experiments was quite complex as it included a system of flow recirculation aimed at preventing water piling-up leeward of the structure. A large number of wave conditions was tested. Two crest widths were tested but only the wide-crested structure, which induces wave breaking, is examined here. As the water depth in the wave flume was varied and the structure height stayed unchanged, the influence of the structure freeboard can be investigated.

The paper is organized in three sections. First, the main features of the numerical model, mathematical formulation, boundary and initial conditions, wave generation method, computational domain, free surface tracking method and numerical resolution scheme, are briefly presented. Then the laboratory tests are described, including experimental set-up, instrumentation and wave characteristics. The third section is dedicated to the results of the numerical simulations. The model is first calibrated and validated by comparing with experimental data, and the numerical information is used to investigate the effect of the recirculation system and the influence of the structure freeboard on the flow conditions.

2. Description of the numerical model

The present study uses the COrnell BReaking waves and Structures (COBRAS) model, whose main features are summarized in this section. The original model, named RIPPLE and developed at Los Alamos National Laboratory (Kothe et al., 1991), is a general program for two-dimensional, transient, free surface incompressible fluid dynamics. It has been modified at Cornell University to deal specifically with coastal engineering issues, in particular breaking wave action and flow within porous media. Details can be found in Lin (1998), Lin and Liu (1998, 1999), Liu et al. (1999, 2000) and Hsu et al. (2002).

2.1. Mathematical formulation

The COBRAS model solves the 2DV Reynolds Averaged Navier–Stokes (RANS) equations, based on the decomposition of the instantaneous velocity and pressure fields into mean and turbulent components. Reynolds stresses are closed with an algebraic non-linear k–ε turbulence model, which can solve anisotropic-eddy-viscosity turbulent flows. The direct resolution of the flow field inside the porous media is not practical, given the complex structure of porous materials. Consequently, the flow in the porous structure is described in the COBRAS model by the Volume-Averaged Reynolds Averaged Navier–Stokes (VARANS) equations, obtained by integration of the RANS equations in a control volume larger than the pore structure but smaller than the characteristic length scale of the flow (see Hsu et al., 2002). Another set of k–ε equations similar to the previous one is used to model turbulence production–dissipation within the porous media.

2.2. Boundary and initial conditions

The boundary conditions for the mean flow field consist of a no-slip condition at the solid boundaries and a zero-stress condition at the free surface. With respect to the turbulence field, a log-law distribution of the mean tangential velocity in the turbulent boundary layer is considered near the solid boundary, where the values of k (turbulent kinetic energy) and ε (dissipation rate of turbulent kinetic energy) can be expressed as functions of the distance from the solid boundary and the mean tangential velocity outside the viscous sublayer. On the free surface, the zero gradient boundary conditions for both k and ε are based on the assumption of no turbulence exchange between the water and air. The initial condition consists of a still water situation, with no wave or current motion.

2.3. Wave generation

The COBRAS model includes a procedure of wave generation using an internal wave maker. The method consists of introducing a source function in the continuity equation for a group of cells defining the source region. The free surface above the source

region responds to a pressure increment defined within the source region cells, and a train of surface gravity waves is generated. See Lin and Liu (1999) for more details. A sponge-layer method, as proposed by Israeli and Orszag (1981), is used to absorb the waves that propagate in the direction opposite the zone of interest, with an imposed exponential damping law.

2.4. Computational domain and free surface tracking method

The computational domain in the COBRAS model is discretized in rectangular cells. The computing mesh can be divided into submesh regions, which allows a variable cells spacing: a finer grid can be defined for the representation of specific study zones. The free surface is tracked using the Volume Of Fluid (VOF) method developed by Hirt and Nichols (1981) that identifies the free surface location tracking the density change in each cell. Besides, the model allows the definition of flow obstacles using a partial cell treatment. See Lin (1998) for further information.

2.5. Numerical resolution

The Reynolds equations are solved using a finite differences two-step projection method (Chorin, 1968). A complete description of the numerical resolution process can be found in Lin (1998).

3. Description of the laboratory experiments

The laboratory experiments described here are part of the research carried out for the European Project DELOS "Environmental DEsign of LOw Crested Coastal Defence Structures". The objective of these experiments is to provide calibration data for numerical and empirical models of flow and stability. The following description is summarized from the corresponding DELOS technical report by Vidal et al. (2001).

Table 1
Characteristics of the gravels used for the models

	W_{15} [g]	W_{50} [g]	W_{85} [g]	Porosity	Density [kg/m^3]
Armour	119	153	206	0.53	2647
Core	3.14	4.31	5.60	0.49	2607

3.1. Experimental set-up

The experiments were carried out in the wave and current flume of the Coastal Laboratory of the University of Cantabria. The wave flume is 24.05 m long, 0.60 m wide and 0.80 m high and is divided, as can be seen in Fig. 1, in different zones. The piston-type wavemaker has two attached free surface wave gauges integrated in an Active Wave Absorption System (AWACS®) that allows the absorption of reflected waves. The wavemaker and the rear absorbing beach occupy 4 m at one of the ends of the flume. The following 4 m are occupied by a false bottom that can be partially or totally removed to set off a current in the flume. The current generation system is a reversible pumping system including two zones of flow injection or sink through the bottom of the flume, two pumps, with a combined maximum discharge of 150 l/s, and a recirculation pipe. The remaining 16 m of the flume are available for the testing of models.

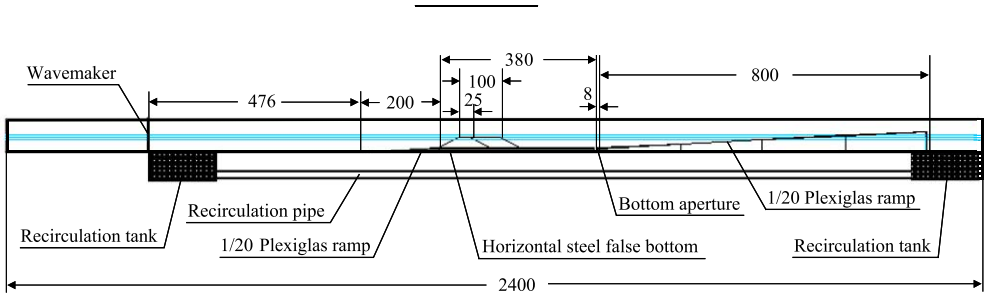

Fig. 1. Definition sketch of wave flume. Experimental set-up.

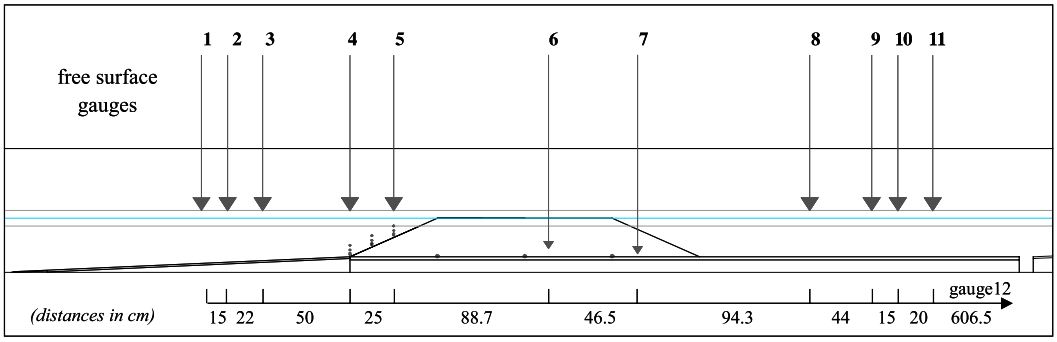

Fig. 2. Instruments and measurement points around and inside the structure.

Bottom and side walls of the testing area are made of glass, allowing the use of laser velocimetry techniques.

Two rubble-mound low-crested structures of 0.25 and 1.00 m crest width, were tested. Crest elevation from the bottom (0.25 m), front and back slope angles (1V/2H) and rubble characteristics were maintained constant for both structures. The models had a two-layer armour of selected gravel and a gravel core. Armour and core characteristics are shown in Table 1.

The low-crested structure model was built over a 3.8-m-long stainless steel horizontal false bottom, 0.10 m over the glass bottom of the flume, Fig. 1. In the frontal foot of the rubble, a Plexiglas ramp with a 1V/20H slope connected the false bottom with the bottom of the flume. In the rear end, another 8-m 1V/20H Plexiglas ramp simulated the rear beach, working as an energy dissipator in order to minimize the effects on the model of the waves reflected at the end of the flume. Between the horizontal and the inclined false bottom, one rectangular aperture, 0.08 m wide, allowed the water to flow below the beach to the return piping system. When the waves piled off water behind the breakwater, the head drove the returning flow through the piping system to the false bottom in front of the wavemaker, thereby closing the circuit. In other words, the pumping system was not activated and the return flow system was only forced by gravity.

3.2. Instrumentation

Among the whole set of gauges and instrumentation installed in the flume, the data used for the present study were measured by 13 resistive free surface gauges to assess free surface evolution, three pressure gauges inside the structure rubble and 12 Laser Doppler Velocimeter measurement points. Three free surface gauges were installed on the slope in front of the LCS to separate incident and reflected waves, Fig. 2. Another two free surface gauges were located over the front slope of the structure at the

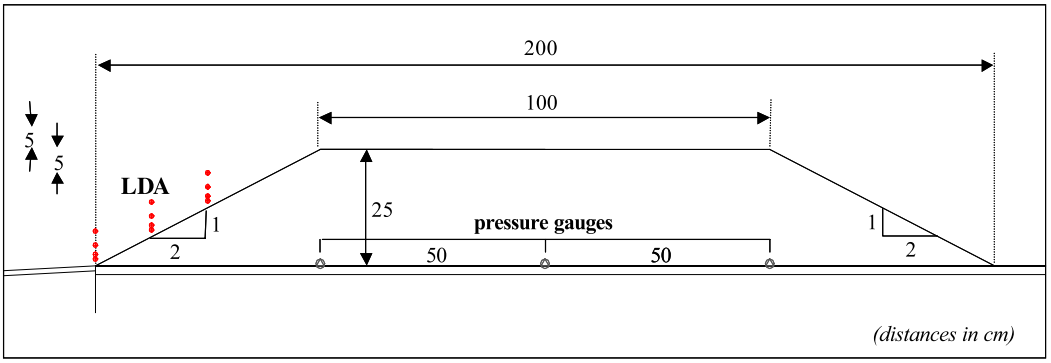

Fig. 3. Close-up of the instruments over and inside the structure.

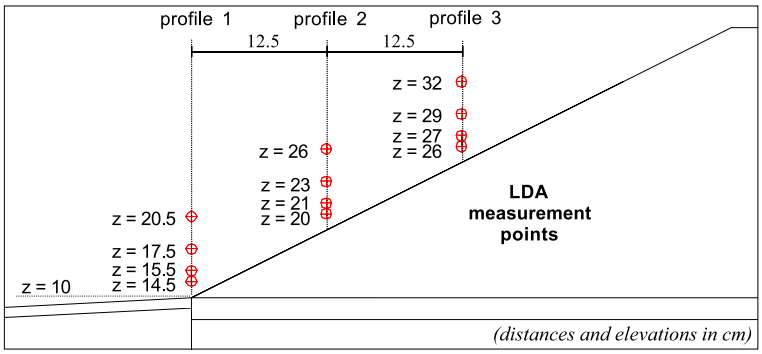

Fig. 4. LDA measurement points location. Front side of the structure.

same x-locations of two of the LDA measurement profiles. Two free surface gauges were placed over the structure crest and on the leeside slope. Four more were placed to measure transmitted waves along the flat bottom behind the LCS. Finally one was installed on the final beach slope. The pressure gauges, see Fig. 3, were installed on the bottom, inside the LCS structure core, to measure the wave transmission inside the rubble mound. LDA measurement points are shown in Fig. 4.

3.3. Wave tests

Two different models (0.25 and 1.00 m crest width) were tested for three different water depths (0.30, 0.35 and 0.40 m) or three different freeboards (−0.05, 0 and 0.05 m). Regular and random waves were tested. The total number of different wave conditions was 54 for both regular and irregular waves for a total of 108. The present study will focus exclusively on the interaction of regular waves with the wide-crested breakwater model. Target wave conditions are indicated in Table 2.

Table 2
Target parameters for generated waves

Wave type		regular
Wave height	H [m]	0.05, 0.10, 0.15
Wave period	T [s]	1.6, 2.4, 3.2
Water depth at wave paddle	h [m]	0.30, 0.35, 0.40
Wave length at wave paddle	L [m]	2.53 to 6.17
Wave steepness	H/L	0.0081 to 0.0593
Relative freeboard	F/H	−1.00 to 1.00
Relative crest width	B/L	0.1621 to 0.3953
Relative wave height	H/h	0.125 to 0.500
Relative depth	h/L	0.0586 to 0.1580

4. Numerical simulations

In this section the numerical model calibration and validation are presented and the main aspects of wave interaction with low-crested breakwaters investigated.

First the computational mesh is described and then the results of the numerical simulations are presented. The first part of the results presentation is dedicated to the model calibration, carried out with one selected test. The model validation consists then of the comparative analysis of the experimental observations with the numerical results for different wave conditions. Once validated, the numerical information is used to investigate the influence of the flow recirculation system and the structure freeboard on the flow pattern.

4.1. Mesh description

The computational mesh designed for the numerical simulation of the experiments described in Section 3 is presented in Fig. 5. The vertical and horizontal axes of the sketch are not scaled. As can be seen, the general configuration of the tests is reproduced. It includes the low-crested structure made of two porous layers of different hydraulic properties, the false bottom supporting the breakwater and connected to the bottom of the flume by a 1/20 slope and the final dissipative 1/20 slope. The return flow system is also reproduced: it consists of a pipe set under the flume and three apertures allowing the water to flow under the final beach, then through the pipe and finally back to the flume right in front of the wave generation zone. As in the laboratory, the returning flow in the numerical flume is exclusively forced by

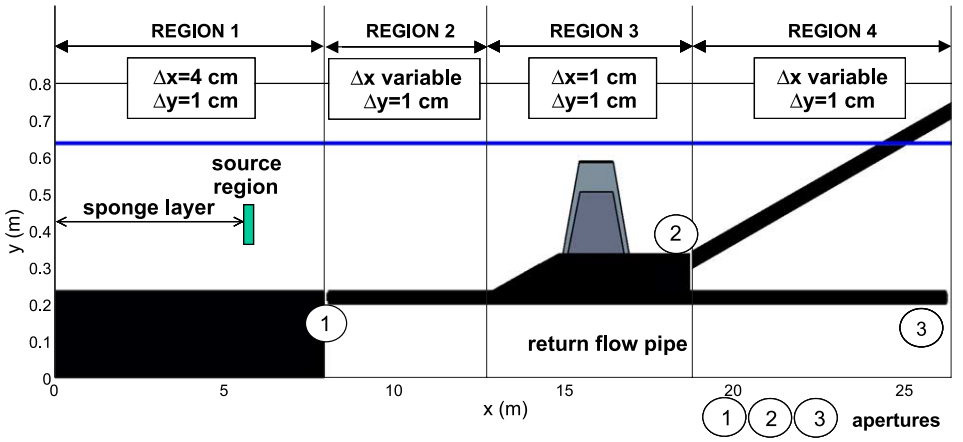

Fig. 5. Sketch of the computational mesh (axes not scaled).

the difference of water level between the seaside and leeside parts of the breakwater. No artificial forcing is included.

The mesh is formed by four submesh regions with different grid sizes. The grid is uniform in the y-direction, but in the x-direction the cell dimension varies from 4 cm in the generation region, without high resolution requirements, to 1 cm in the vicinity of the structure which is the zone of interest. The model's ability to deal with nonuniform meshes allows considerable savings of computational time. Waves of different periods are modelled with different meshes, according to the rules of thumb for the design of the wave generation zone proposed by Lin (1998). The total number of cells is 80 in the y-direction and varies in the x-direction from 1290 for the short waves propagation up to 1749 in the case of the longest waves.

4.2. Model calibration/validation

The first step of the numerical simulations consists of the calibration of the model, specifically the calibration of the α and β parameters governing the flow inside the porous structure. The model calibration was carried out using a reference test with the following wave conditions: h=40 cm, H=7 cm, T=1.6 s. The 40 cm water depth at the wave paddle is the maximum of the three tested in the present set of experiments. Thus, the 25-cm high structure, built on a 10-cm high false bottom, is submerged, with a negative 5 cm freeboard.

The low-crested structure modelled in the present study is not a homogeneous reef-type breakwater. It is formed of an armour and a core with different grain sizes and porosities, and thus different magnitudes of the associated frictional forces for a given flow. As a consequence, two pairs of α and β parameters, accounting for linear and nonlinear drag respectively in each of the porous layers (see Hsu et al., 2002, for equations and nomenclature), are to be calibrated. A series of computations and comparisons with measurements was conducted with that objective, considering previous results from Shih (1990), Van Gent (1994, 1995), Van Gent et al. (1994), and Burcharth and Andersen (1995) to estimate the range of possible values. The calibration has been conducted comparing the measured and the computed values of free surface displacement at different sections all along the flume (see location of the wave gauges in Fig. 2) and led to the following results: α is taken to be equal to 1000 for both the armour layer and the core, and β equal to 0.8 and 1.2, respectively. As will be seen later, the comparison of the measured and computed pore pressure time series and mean velocities at the seaside slope of the breakwater shows satisfactory results and confirms the values of the porous media parameters resulting from the free surface calibration as the optima. Parameters were kept constant for any wave conditions in order to check the model predictive capability. The results of the model calibration are presented in the following figures.

Fig. 6 shows the maximum and minimum wave height envelopes and the mean water level measured

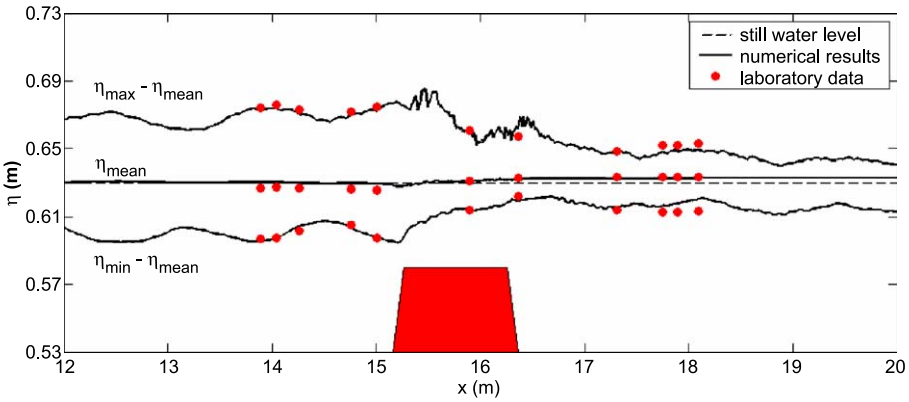

Fig. 6. Wave height envelopes and mean water level. h=40 cm, T=1.6 s, H=7 cm.

in the laboratory (dots) and calculated with the numerical model (solid lines). Numerical data result from a 10-wave phase-averaging, counted from 60 s of simulation to ensure stabilized flow conditions. As can be seen in this figure, the agreement between experimental and numerical data is very good. The model is able to simulate adequately the main features of the propagation of a wave train passing over a submerged breakwater. In terms of wave height envelopes, the whole pattern is accurately computed. Reflection on the rising front of the structure induces a partial standing wave system in the seaward region that the model is able to reproduce well. In the region of the structure crest, the wave height damping due to breaking and percolation inside the porous layer is correctly fitted. In the leeward region, the transmission pattern due to overtopping and flow through the structure is well reproduced, though the maximum wave height at the last gauges is slightly underpredicted. A modulation of the wave amplitude can also be observed in the transmission zone, due to partial reflection on the final ramp (the reflection coefficient is about 20%) and release of higher order frequency components as commented further. The wave breaking-induced mean water level variations can be clearly observed and are well reproduced by the model: the mean water level decreases at the offshore side of the breaking point and then increases at the onshore side. Besides, overtopping of the structure induces in the leeward zone an increase of the mean water level, of utmost importance in the dynamics of this region. As can be seen in the figure, this set-up is correctly computed.

Fig. 7 displays the time series of the free surface displacement for each one of the free surface gauges presented in Fig. 6, and also for gauge 12 located in the surf zone of the final beach. The solid line corresponds to the measurements and the dots to the numerical results.

The total set of free surface gauges can be divided into three groups representing the different hydrodynamic zones of the breakwater vicinity. As described in Section 2, gauges 1 to 5 are located seaward of the structure, the first three on the offshore slope and the following two on the front face of the breakwater. The second zone corresponds to the structure crest, where wave breaking occurs. Free surface evolution over the crest is recorded at gauge 6. Finally, time series at gauges 7 to 12 characterize the transmission zone. Gauge 7 is located just on the structure leeside slope and gauge 12, as mentioned above, over the dissipative slope at the end of the flume. As can be seen, the model is able to reproduce very well the free surface time history for each one of the three regions. The incident wave train propagates on the initial gentle slope (gauges 1 to 3), then deforms and becomes more asymmetric while interfering with the rising front of the breakwater (gauges 4 and 5) until reaching an unstable situation. Then the relative crest width (crest width divided by wave length) is large enough to make the waves break over it (gauges 6 and 7). As can be seen, the use of the Volume Of Fluid technique enables the COBRAS model to reproduce with accuracy the free surface during and after wave breaking, where other numerical models for breaking waves fail to calculate the

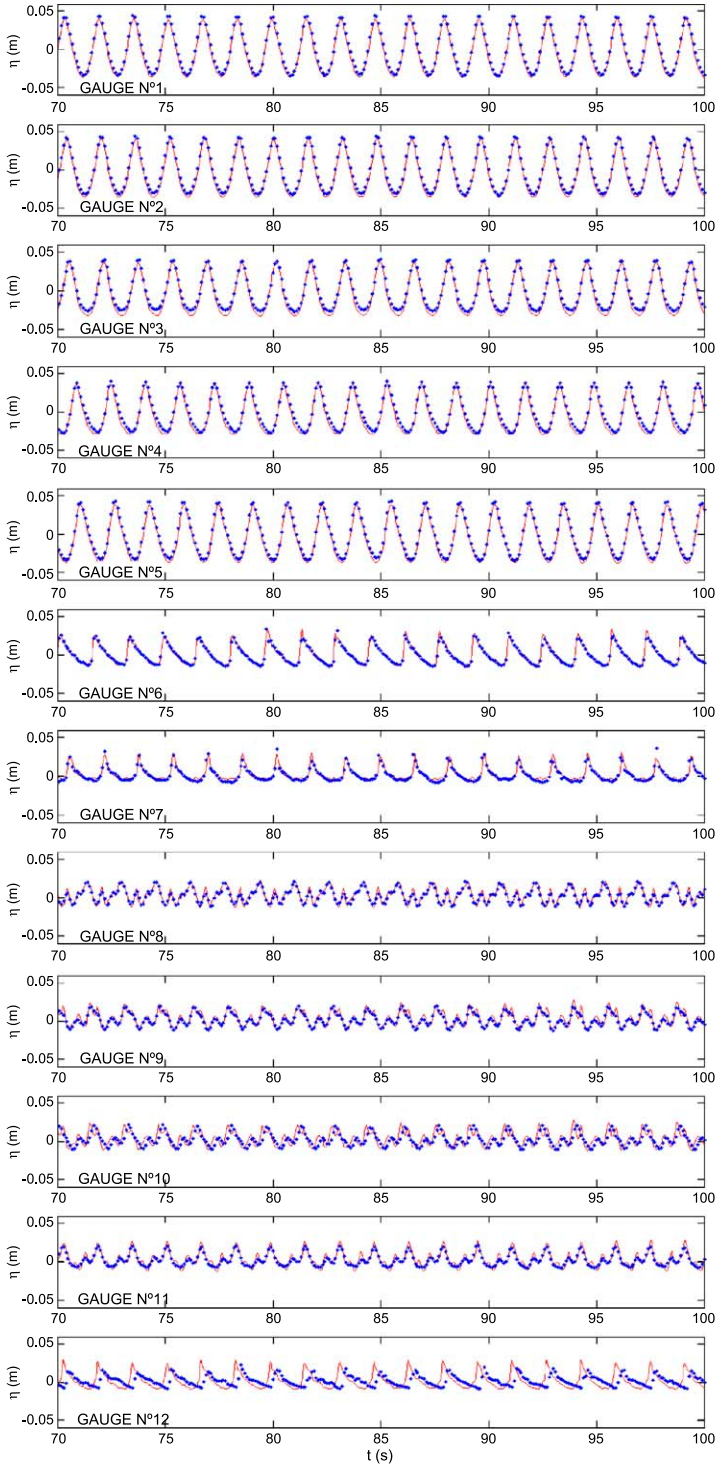

Fig. 7. Free surface time series, gauges 1 to 12. h=40 cm, T=1.6 s, H=7 cm. Solid lines: experimental dat. Dots: numerical results.

free surface. Furthermore, the VOF technique combined with RANS equations does not require the introduction of a specific breaking criterion to target wave breaking.

Wave records in the transmission zone (gauges 8 to 11) show a complex profile that the numerical model reproduces adequately. This complex wave shape, with multiple crests, accounts for the higher harmonics generation over the submerged breakwater. Nonlinear phenomena of wave–structure interaction result in the amplification of bound waves (phase-locked with the first harmonic) that are released when breaking occurs over the structure crest. In the deeper waters leeward of the obstacle, the phenomenon known as wave decomposition takes place, as the free waves propagate at a different celerity than the primary wave, and gives rise to a spatial modulation of the transmitted wave amplitude. This phenomenon has been observed in many experimental and numerical studies like Beji and Battjes (1993) and Beji and Battjes (1994), or in field experiments by Masselink (1998) or Sénéchal et al. (2002), and for waves propagating over a porous step by Losada et al. (1997).

The energy transfer from the fundamental harmonic to higher frequencies is illustrated in Fig. 8. The amplitude of the first five harmonics at each one of the gauge stations is represented for both numerical and experimental cases. The model reproduces the laboratory data with a good level of agreement. The maximum error on the first two harmonic amplitudes is 10% at station 7 and 14% at station 5 respectively. The rate of error is greater for the higher frequency components, but the corresponding amplitudes are too small (one or two orders of magnitude with respect to the first harmonic at the first six stations) for the error to be significant. At station 6, the first harmonic amplitude abruptly decreases as breaking occurs over the structure crest, coinciding with an enhancement of higher harmonics amplitude. Previously, at station 5, the fundamental harmonic amplitude increases as a result of the shoaling effect on the front side of the structure.

Once the model is calibrated in terms of free surface displacement, the numerical data are directly compared with the dynamic pressure measured inside the porous structure. The comparison between meas-

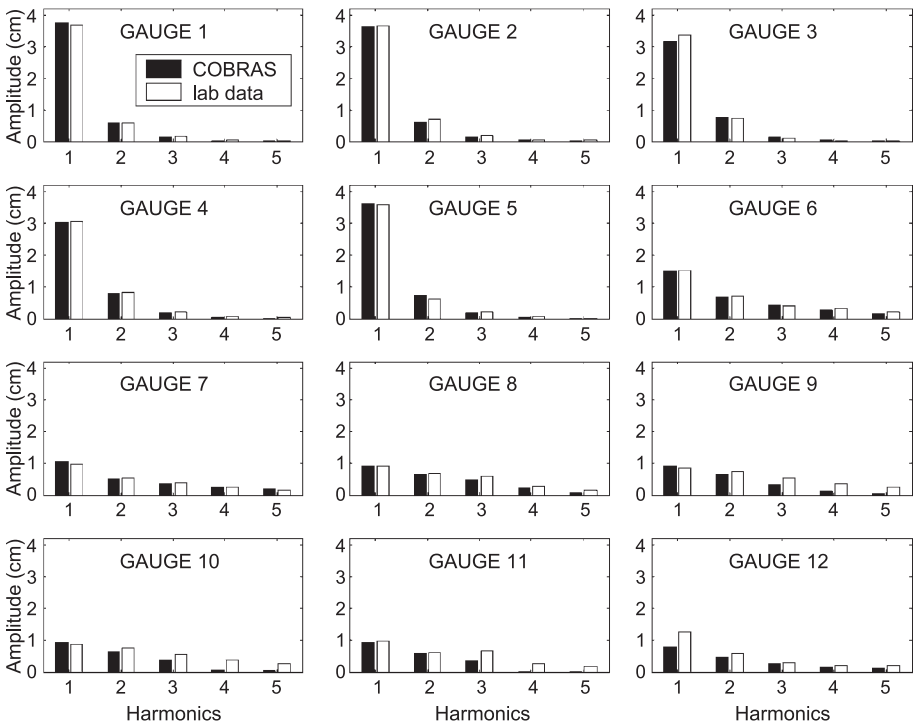

Fig. 8. Harmonics amplitude, gauges 1 to 12. h=40 cm, T=1.6 s, H=7 cm.

ured and computed time series of the pressure at the three stations located inside the structure, at the interface with the steel false bottom (see Fig. 3), is presented in Fig. 9. As can be seen, the computed pressure time series agree favourably with the corresponding measurements. The same behaviour as free surface in terms of wave attenuation can be observed: the instantaneous pressure decreases along the structure, from the exposed front slope of the breakwater to the leeside slope.

In addition to free surface displacement and pore pressure, particle velocities at the seaward slope of the structure were considered in the calibration process. The estimation of the velocity field in the vicinity of the breakwater is of utmost importance, for instance, as a first step in the analysis of the stability of the structure. Fig. 10 shows, for each one of the three profiles of measurements presented in Fig. 4, the phase-averaged horizontal and vertical velocities vs. time normalized with the wave period. The first and second lines of the graphs correspond to horizontal and vertical velocities, respectively, while the four columns correspond to the different elevations of measurement points. Solid and dashed lines represent experimental and numerical data, respectively. As can be seen, the agreement is rather good, in terms of amplitude and wave profile. The highest discrepancies appear at profile 1, at the point nearest to the structure bottom (z=14.5 cm), where local effects of the stones are the most likely to perturb the measurement. It has to be pointed out that obstacles in the computational domain are defined through a partial cell treatment allowing the obstacles slopes to intersect the cells and not to be saw tooth-shaped. As a result, the numerical model deals with a smooth-faced breakwater while measurements in the laboratory are taken on a rubble-faced structure.

The tests simulated with the same water depth (h=40 cm) but with different wave heights and periods show no great influence of these variables on the model performance. The coefficients α and β are kept constant and are not used as adjusting parameters for each of the different tests. Fig. 11 shows the results of wave height envelopes and mean water level for different wave conditions. Fig. 11a and b correspond to higher (10 cm wave height) and smaller (3.6 cm) waves, respectively, than in the previous case (7 cm), with the same period (1.6 s). Influence of the wave period can be appreciated by comparing Fig. 11b to d, corresponding to 1.6, 2.4 and 3.2 s wave periods, respectively, for the same wave height. For all these cases, the wave field around the submerged breakwater is well reproduced by the numerical model. In the case of the largest incident waves, the discrepancies between experimental and numerical data are more pronounced, especially for the maximum wave

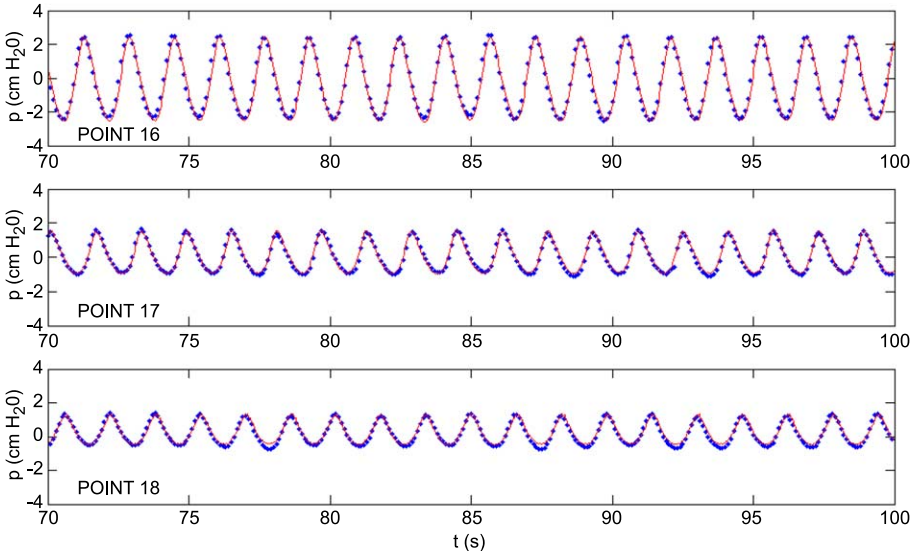

Fig. 9. Pressure time series. h=40 cm, T=1.6 s, H=7 cm. Solid lines: experimental dat. Dots: numerical results.

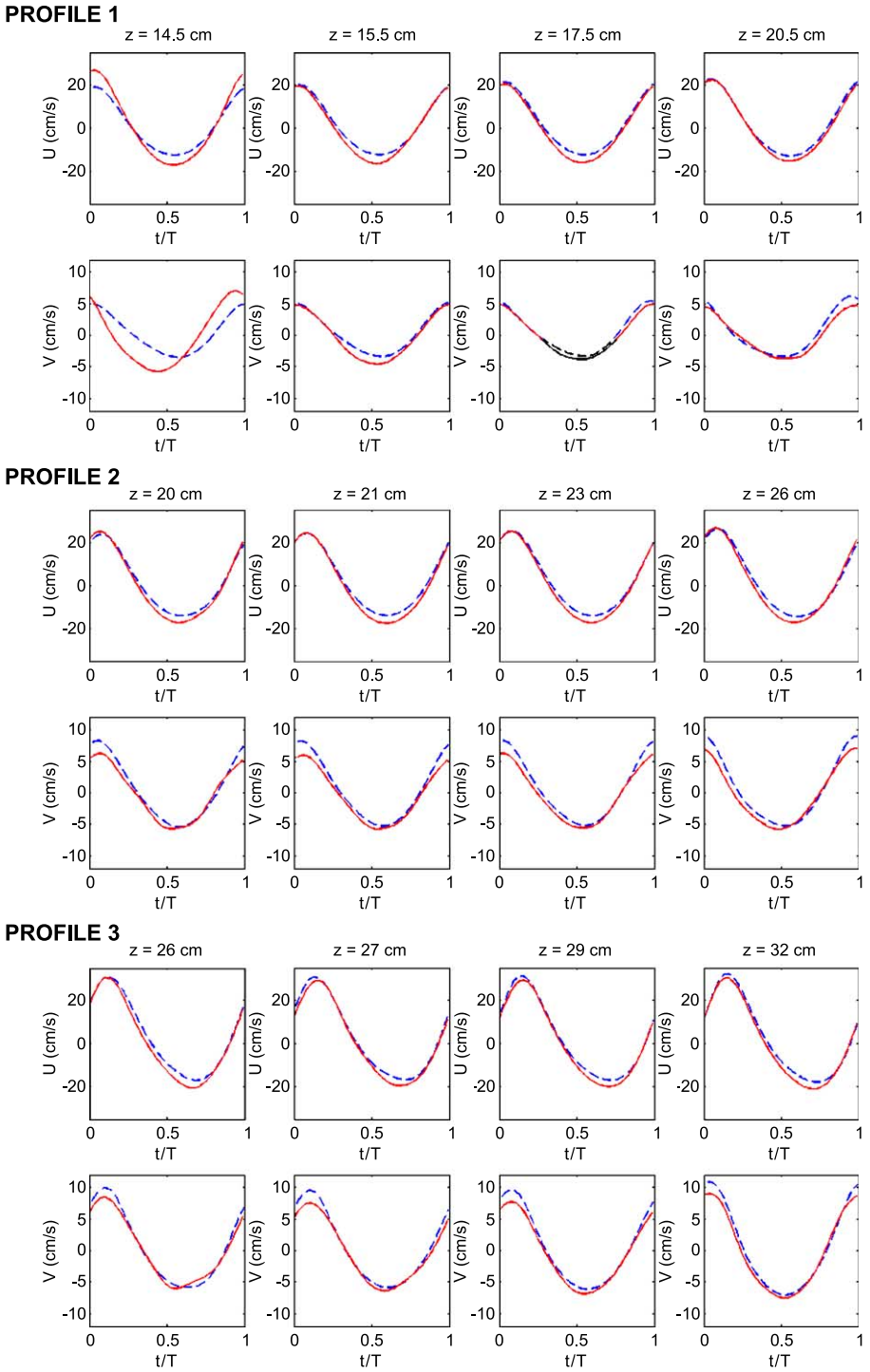

Fig. 10. Phase-averaged velocities. h=40 cm, T=1.6 s, H=7 cm. Solid lines: experimental data. Dashed lines: numerical results.

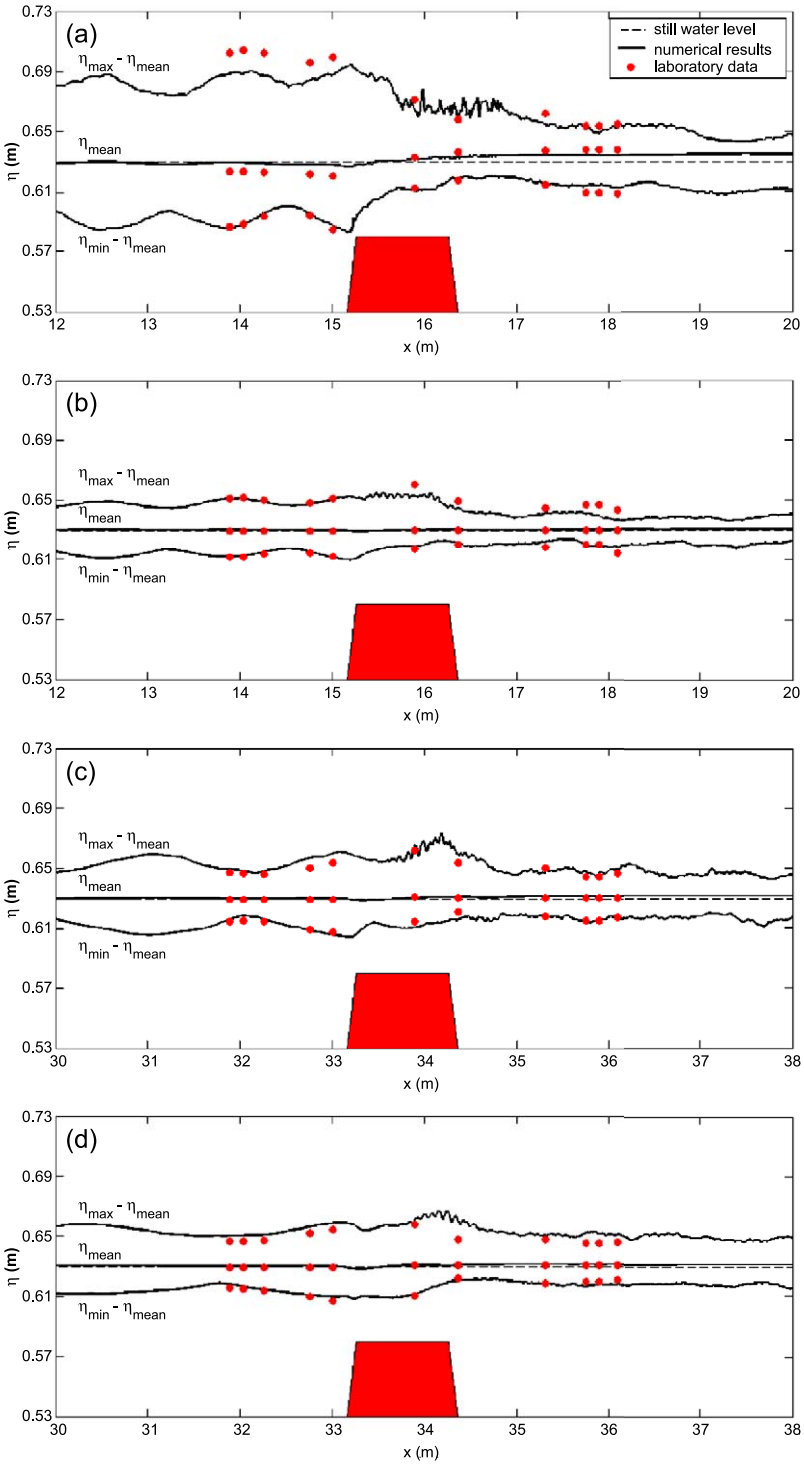

Fig. 11. Wave height envelopes and mean water level. (a) h=40 cm, T=1.6 s, H=10 cm. (b) h=40 cm, T=1.6 s, H=3.7 cm. (c) h=40 cm, T=2.4 s, H=.37 cm. (d) h=40 cm, T=3.2 s, H=3.7 cm.

height envelope which is quite overestimated seaward of the structure. This is due to the fact that the selected values for α and β are not optima for the high Reynolds number flow conditions induced by this extreme value of wave height, about three times the wave height of cases (b) to (d). The small discrepancies in the transmission zone observed in the simulation of the shortest waves (Figs. 6 and 11a,b) are reduced when wave period is increased. Wave breaking is clearly different compared to the previous case, turning from collapsing for high and intermediate waves to spilling in the case of the smallest waves. An increase in wave period moves the breaking point in the onshore direction. The short waves break over the very beginning of the crest zone, while breaking of the longer waves occurs at the landward limit of the crest zone.

As a first conclusion, the model is proven to simulate the hydrodynamic behaviour of a submerged structure with a high degree of agreement with experimental observations. The values of the porous media parameters set for the simulation of H=7 cm, T=1.6 s waves, are validated and are proven to give satisfying results independently of the wave height and period. It is important to point out that the results presented in Fig. 11 can be improved and the commented discrepancies removed by adjusting the porous media parameters depending on the wave conditions. Nonetheless, the objective of the present calibration is to fit the breakwater response using constant values of these porous media parameters for any conditions of flow, in order to show the model's ability as a predictive tool.

Therefore, in contrast with previously existing models for wave interaction with permeable low-crested structures, it can be said that the model performs reasonably well for all the magnitudes considered, i.e. wave envelopes, free surface evolution, velocities and pressure, and for different incident wave conditions.

4.3. Analysis of results

In this section, three additional tests are presented and compared with the reference test (h=40 cm, H=7 cm, T=1.6 s) included in the previous section. The corresponding numerical simulations are mainly used to investigate two important aspects. First, the influence of the recirculation system described in Section 3 on the near-structure flow conditions is studied. Next, the influence of the freeboard is considered and results of wave interaction with zero and positive freeboard structures are presented. These aspects are studied based on a combination of experimental and numerical results. As will be shown, one of the main advantages of the model is the possibility of numerically reproducing several magnitudes that either cannot be measured or require an intensive and expensive experimental programme.

4.3.1. Influence of the return flow system

Low-crested structures are by definition strongly overtopped structures, designed to allow the transmission of a certain amount of the incident wave energy. In most 2-D laboratory experiments on this type of structures, the overtopping gives rise to a piling-up of water in the leeside region of the structure and hence to an increase of the mean water level pointed out, for instance, by Loveless and Debski (1997). This set-up in the transmission zone modifies the dynamics of the waves reformed in this region and the flow conditions in the vicinity of the breakwater. It forces a strong return flow over the structure which perturbs the wave breaking process on the structure seaward slope and crest, influencing the breaker type, position and height. In real cases of stretches of shore protected by low-crested structures, this phenomenon is not observed, as the potential piling-up behind the breakwater is relieved by 3-D circulation systems. Part of the flow is transmitted back to the seaward side through the permeable structure, but a greater proportion returns to the open sea by the sides of the breakwater, following pathways of lesser resistance. The configuration of the laboratory tests conducted for this study has been thought to prevent this usual shortcoming of 2-D experiments consisting of a non-realistic set-up leeward of the low-crested breakwater.

To examine the influence of the flow recirculation system, a laboratory test without recirculation was conducted, with the same wave conditions as the reference test. Thus the structure considered in this test is submerged, with a negative 5 cm freeboard. Fig. 12 shows the results of surface elevation envelopes and mean water level when no flow recirculation is considered. The same high degree of

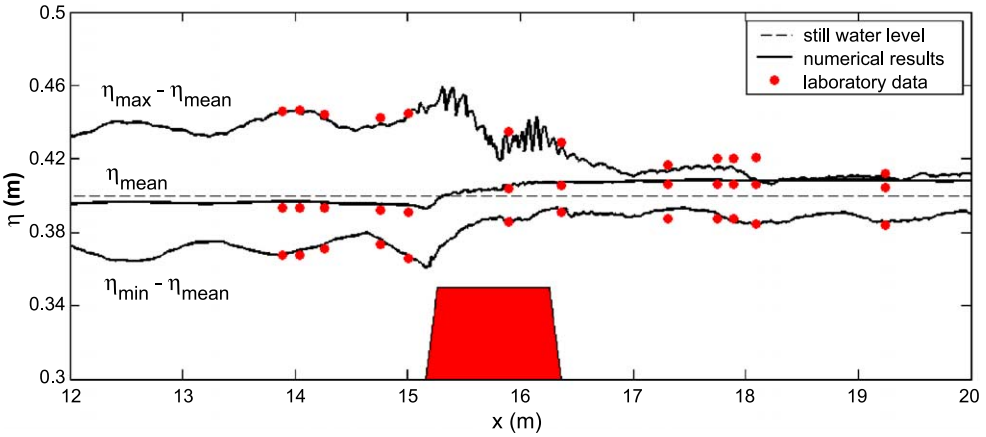

Fig. 12. Wave height envelopes and mean water level. h=40 cm, T=1.6 s, H=7 cm. No flow recirculation.

agreement between experimental and numerical data is obtained as for the equivalent test including flow recirculation. The wave height patterns at both sides of the structure are well tracked: the model adequately reproduces the breakwater performance in terms of reflection and transmission. The set-down previous to wave breaking above the seaside slope of the structure and the post-breaking set-up in the leeward zone are adequately simulated. The excessive value of the set-up in the transmission region due to overtopping as commented earlier is correctly predicted.

It can be seen that the mean water level in the leaward zone is significantly higher in the case where recirculation is not allowed compared to the reference test. Wave height envelopes in the transmission zone, as well as wave breaking over the structure crest, are also influenced by the flow recirculation system. Thus, comparing Figs. 6 and 12, it can be concluded that the flow recirculation system is checked to work properly, in both the experimental and numerical wave flumes.

Fig. 13 clearly demonstrates the influence of the flow recirculation system on the flow structure. The computed mean (ensemble-averaged) flow around and inside the breakwater is plotted, in terms of stream lines and velocity field, for both configurations, without and with recirculation. Mean flow is obtained by averaging over 5 waves starting from instant t=60 s of the simulation.

The mean water level increase in the transmission zone due to overtopping induces a hydraulic gradient and therefore a return flow directed offshore. In the first case where the recirculation pipe is locked, this return flow hinders the onshore transport associated with wave nonlinearity and wave breaking and gives rise to a mean current directed offshore. In the transmission zone, velocities are very low and this mean current can hardly be appreciated. Higher velocities are observed over the crest, where the reduction of the water depth induces an acceleration of the flow, and result in the formation of a vortex cell at the seaward slope of the structure.

In the case of the test including flow recirculation, the excess of water in the leeward zone due to overtopping flows back through the return pipe. This configuration allows mean motions to become well-established and to have a nature-like pattern. The overall transport is directed onshore, and the strong current over the structure crest due to flow constriction and breaking. Flow separation at the crest edge originates the formation of a vortex at the leeside slope. Another vortex cell of smaller dimensions can be observed at the toe of the seaward slope. This vortex influences the stability of the structure as the local offshore velocities are responsible for the well-known scour phenomenon.

The vertical distribution of the mean flow, Fig. 14, illustrates the significant differences between the no-recirculation and the recirculation configurations. Six sections at the breakwater vicinity have been selected and the ensemble-averaged horizontal velocity profiles at these sections have been plotted for both configurations. In the case of no recirculation, the mean current below the trough level is directed

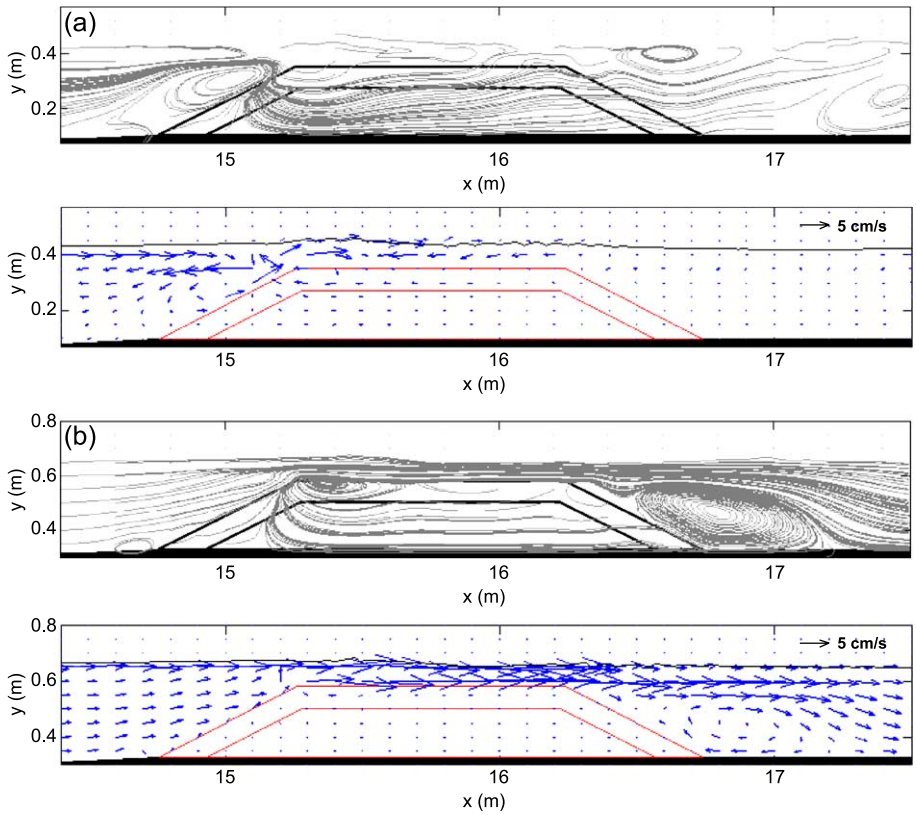

Fig. 13. Computed mean (ensemble averaged) velocities: (a) case without flow recirculation, (b) case with flow recirculation.

seaward, outside and inside the structure. The seaward mean velocities in the transmission zone, as can be observed at Section 12 profile, are found to be very low, with a maximum value of 0.5 cm/s just below the trough level. At Section 6 the vortex cell that forms at the seaward slope results in an inversion of the mean flow and an onshore near-bed component. The breaking process at the seaward edge of the structure crest allows a greater penetration of the flow and higher mean velocities inside the porous medium in this zone, as seen at the Section 7 profile.

When recirculation is allowed (Fig. 14b), the net transport is clearly shoreward. As mean motions are of greater intensity in that case, the horizontal scale has been reduced for reasons of clarity. At Section 6 the profile under the trough level is almost uniform vertically but shows a peak value known as the overshooting effect near the structure. This phenomenon, observed by Lomonaco et al. (2002), consists of an acceleration of the flow, as a result of the reduction of water depth, slightly before the wave crest passes. This local velocity enhancement at the interface with the structure is obviously of great relevance regarding stone stability. Over the structure crest, mean velocities are substantially higher, as a result of flow constriction and wave breaking. Inside the porous structure, these velocities are nearly zero, or slightly negative as a consequence of the vortex cell formed leeward. The two equivalent sections in the transmission zone show significant differences: the low negative values in the no-recirculation case become positive and about six times higher in the configuration with flow recirculation.

As a conclusion, the absence of a flow recirculation system aimed at discharging the overtopping-induced excess of mass leeward of the structure is confirmed to strongly influence the flow pattern in the flume. The flow recirculation system is found to be fundamental in the adequate 2DV modelling of the low-crested structure hydrodynamics. Besides, the

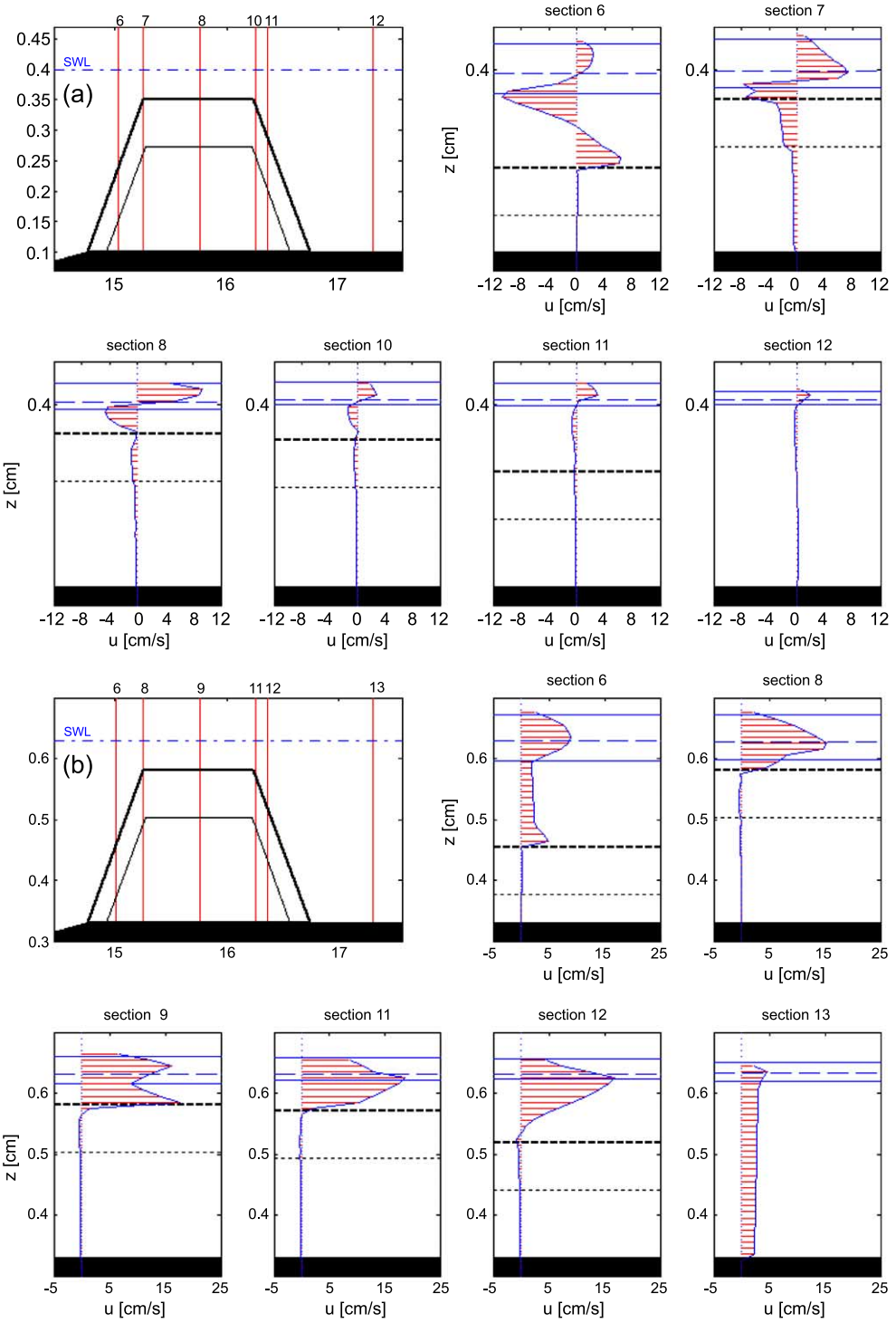

Fig. 14. Computed mean (ensemble averaged) velocities: (a) case without flow recirculation, (b) case with flow recirculation.

COBRAS model is found to be able to deal with the complex laboratory test configuration including the flow recirculation system.

4.3.2. Influence of the structure freeboard

In this section, a similar analysis is carried out to study the influence of the breakwater freeboard F on the flow pattern. As emphasized by D'Angremond et al. (1996), crest elevation relative to still water level is a crucial parameter in wave transmission, along with wave characteristics (height, period, relative depth) and the breakwater type (permeability, surface roughness). In order to analyse the influence of the structure freeboard, two additional cases have been considered, with zero and positive freeboards. Flow recirculation is allowed in both cases. These two cases can be regarded as extreme cases since most of the existing models for wave and submerged or low-crested structure interaction fail to reproduce the flow field under these conditions. However, it has to be pointed out that in meso and macrotidal environments these are two cases to be considered in the design of low-crested structures.

As can be seen, the same high degree of agreement between experimental and numerical data as for the 40-cm water depth tests is obtained. The wave envelope patterns and mean levels at both sides of the structure are well tracked: the model adequately reproduces the breakwater performance in terms of reflection and transmission.

Reflection on the structure seaward slope induces a clear partial standing wave pattern, well reproduced by the model. The same phenomenon takes place leeward of the structure, as the final beach-reflected wave combines with the breakwater-transmitted wave. In the case of the emerged breakwater, the transmitted wave height is too small for this feature to be clearly observed. For the tested wave conditions (H=7 cm, T=1.6 s), the zero freeboard breakwater is slightly overtopped and waves break on the seaward edge of the crest. In the case of the 5 cm freeboard structure, no overtopping occurs; waves break on the upper part of the seaward slope. Transmission only occurs through the porous structure, giving rise to a very low-perturbed landward wave field. In both situations the set-down previous to breaking above the seaside slope of the structure and the post-breaking set-up are correctly simulated.

As pointed out by Burcharth and Andersen (1995), the porous media α and β parameters are flow dependent. Still, in the previous model calibration/validation section, they were kept constant for any wave conditions in order to check the model ability to reproduce the hydrodynamics of the submerged structure. Nonetheless, flow conditions at emerged breakwaters are very different, as will be verified afterwards, and the core nonlinear drag β parameter needs to be adjusted compared with the $F\leq 0$ structure. β equal to 0.4 (instead of 1.2 for negative or zero freeboard structures) was found to better fit the laboratory observations.

The good performance of the model regarding the zero freeboard structure is illustrated in Figs. 16 and 17. Fig. 16 displays the time series of free surface displacement at gauges 3 to 8, all located in the vicinity of the structure (see Fig. 2). The solid line corresponds to the measurements and the dots to the numerical results. All graphs are plotted with the same vertical scale to better visualize the substantial reduction of the wave height. The initial phases of the incident wave train evolution and transformation are the same as for the submerged breakwater: the waves get steeper while passing on the initial gentle slope and then shoals on the seaside slope of the structure. The waves adopt an unstable profile earlier, as the relative depth is smaller, and the breaking point is slightly moved seaward. As the structure crown is higher, the amount of water that overtops it is reduced and the onshore wave field is, therefore, less perturbed. It is interesting to note the model ability to deal with the specific situation of a thin film of water covering the crest of the structure (station 6). Multiple crests in the onshore wave field can be observed: also in the case of the zero freeboard breakwater the model is found to simulate adequately the nonlinear wave decomposition process.

The reduction of wave height and harmonics enhancement can be observed in Fig. 17. Vertical scale is kept constant for all the gauges for an easier comparison. The model calculates the harmonics amplitudes with a reasonably good agreement. From gauge 6, located over the structure crest, wave energy is distributed over a broader range of harmonics. The amplitude of the fundamental harmonic of the incident wave spectrum decreases considerably, as part of the incident energy is

dissipated and another part redistributed to higher frequencies. At station 5 the calculated amplitude of the first harmonic is 96% of its value at station 3. It then decays to 22% in the crest zone (station 6) and to 9% leeward of the structure (station 8). The error on the first harmonic amplitude is less than 6%, except at gauge 7 where the calculated amplitude differs out of 14% from the measured one. However, the error is not very significant as the harmonic amplitude is about 4 mm at this station.

Figs. 18 and 19 correspond to the case of the +5 cm freeboard. As can be seen, the water surface displacement around and inside the emerged breakwater is well reproduced by the model. The same phenomena of wave shoaling and breaking as in the previous cases can be observed, with a slight translation seaward. Wave profile reaches an unstable shape earlier, and breaking occurs between stations 5 and 6, on the upper part of the seaward slope. Surface variations at stations 6 and 7 are recorded inside the porous structure, in the crest and leeward slope regions, respectively. As can be observed, wave energy is considerably damped. The drastic reduction of the incident wave height is clearly illustrated by Fig. 19. At station 5, the calculated amplitude of the first harmonic represents 93% of its value at station 3. This percentage decreases to 17% at station 6 and 5% at station 8. The error between numerical and experimental values is about 10%, except at gauge 8 (32%) but the wave height is lower than 2 mm at this station.

From the results presented in Figs. 15–19, it can be concluded that the model performance is not affected by strong variations of the freeboard. The model is

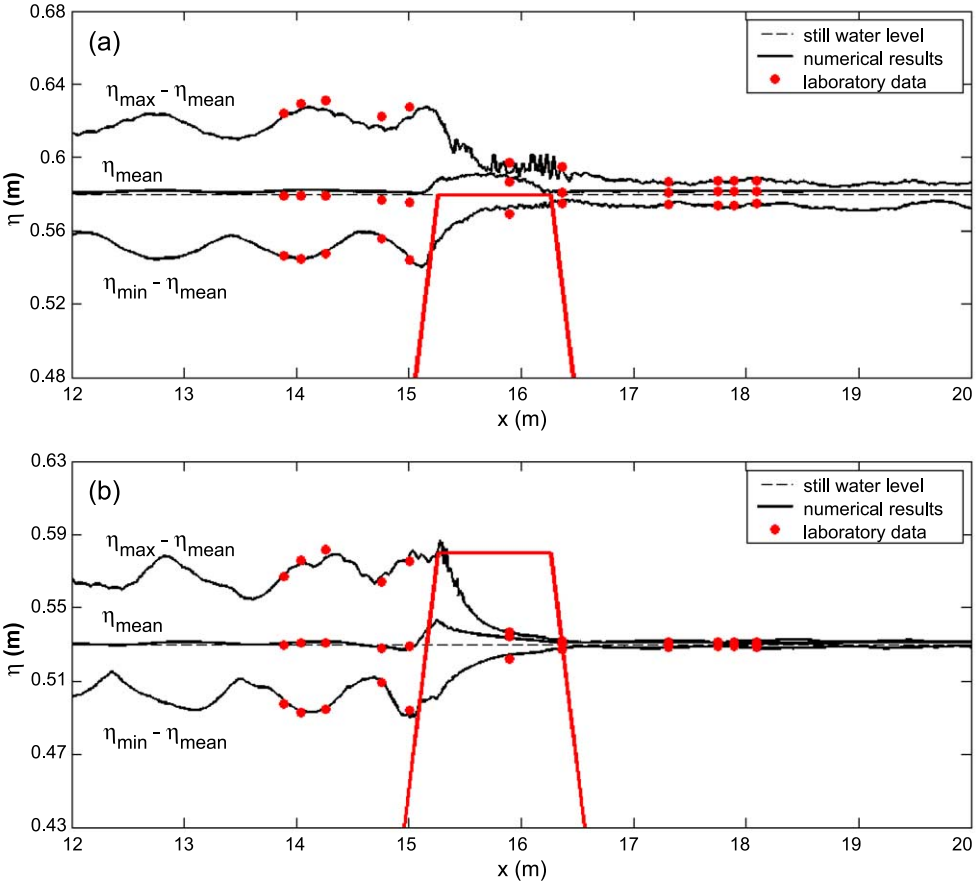

Fig. 15. Wave height envelopes and mean water level. (a) h=35 cm, T=1.6 s, H=7 cm. (b) h=30 cm, T=1.6 s, H=7 cm.

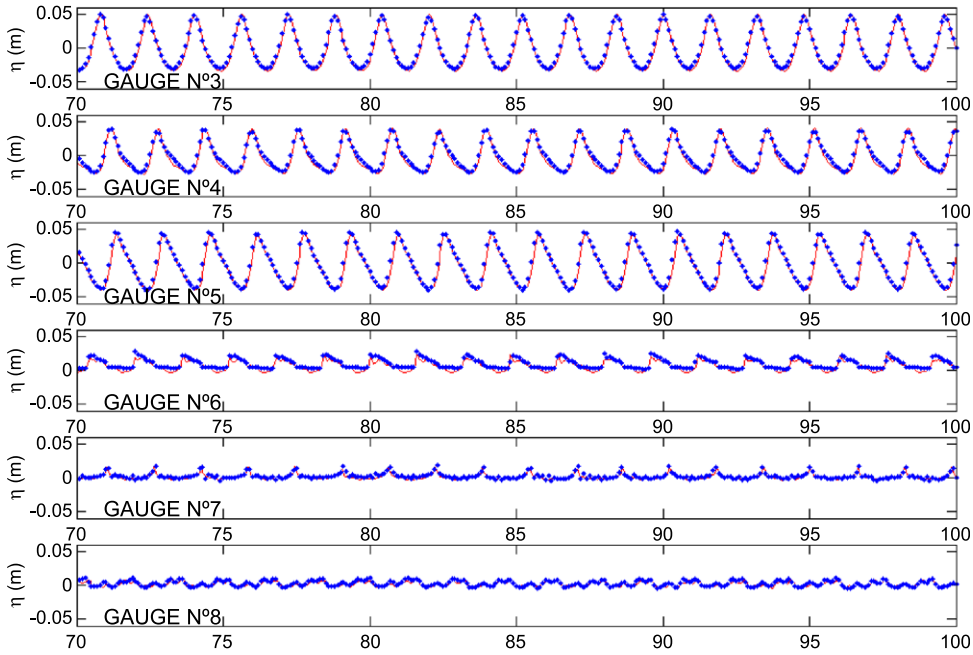

Fig. 16. Free surface time series. h=35 cm, T=1.6 s, H=7 cm. Solid lines: experimental data. Dots: numerical results.

able to simulate the wave interaction with a porous breakwater, whether submerged or emerged, with the same level of accuracy, despite their very different hydrodynamic behaviours. These differences are clearly illustrated by Fig. 20. Snapshots of the velocity field around the structure at 4 different instants are plotted for the three tested freeboards. Wave breaking conditions are obviously affected by the structure

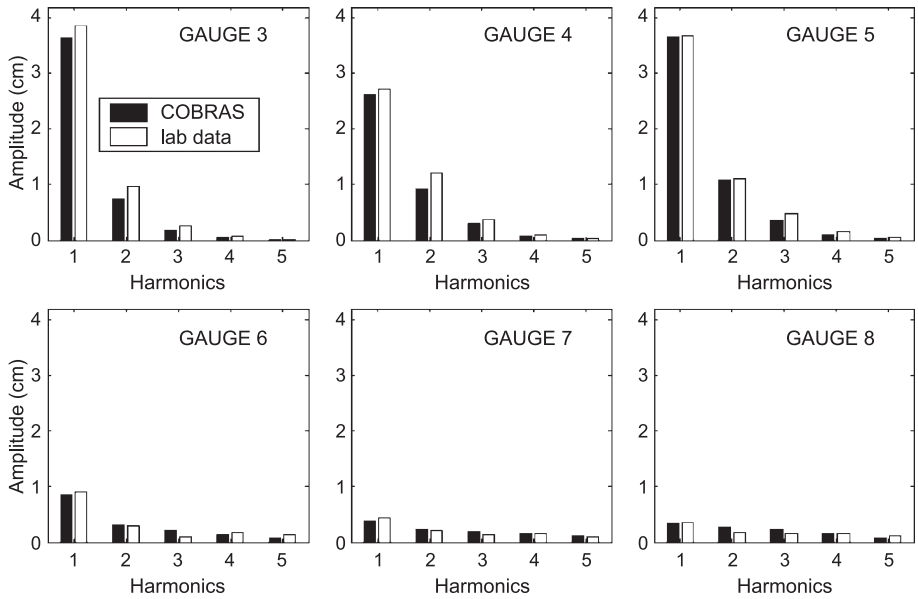

Fig. 17. Harmonics amplitude, gauges 3 to 8. h=35 cm, T=1.6 s, H=7 cm.

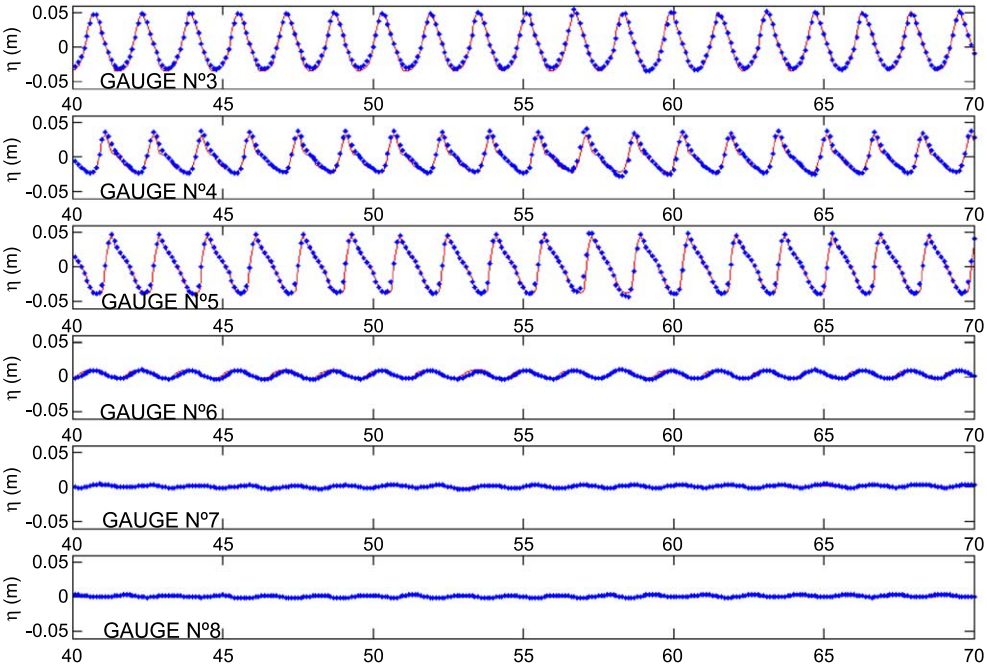

Fig. 18. Free surface time series. h=30 cm, T=1.6 s, H=7 cm. Solid lines: experimental data. Dots: numerical results.

freeboard. Spilling or collapsing breakers over the crest when the structure is submerged turn into collapsing on the crest seaward edge in the case of the zero freeboard, and surging on the seaward slope when the structure emerges. Among the three tested crest elevations, the breaking-induced peak velocities are minimum when the structure is submerged and maximum when the freeboard is zero. The seaward

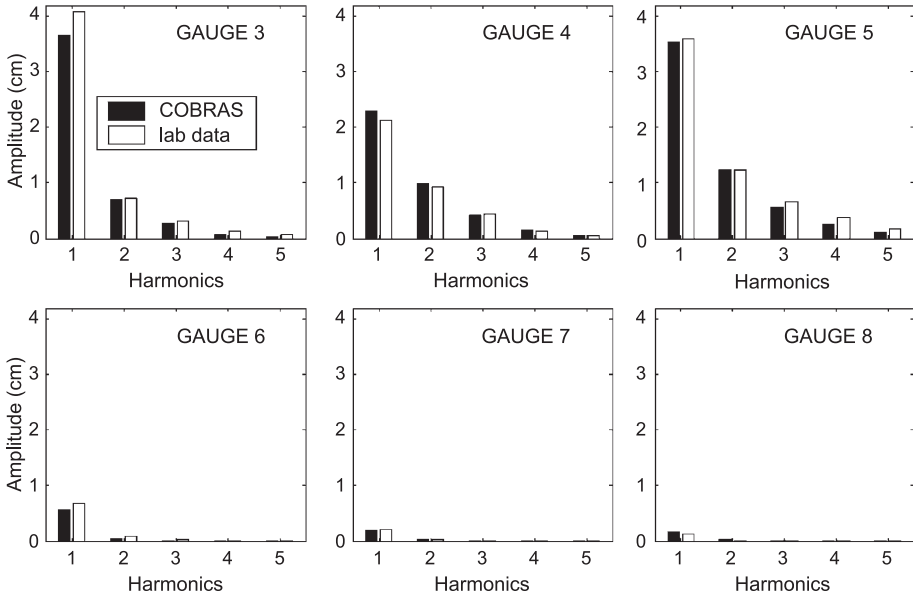

Fig. 19. Harmonics amplitude, gauges 3 to 8. h=30 cm, T=1.6 s, H=7 cm.

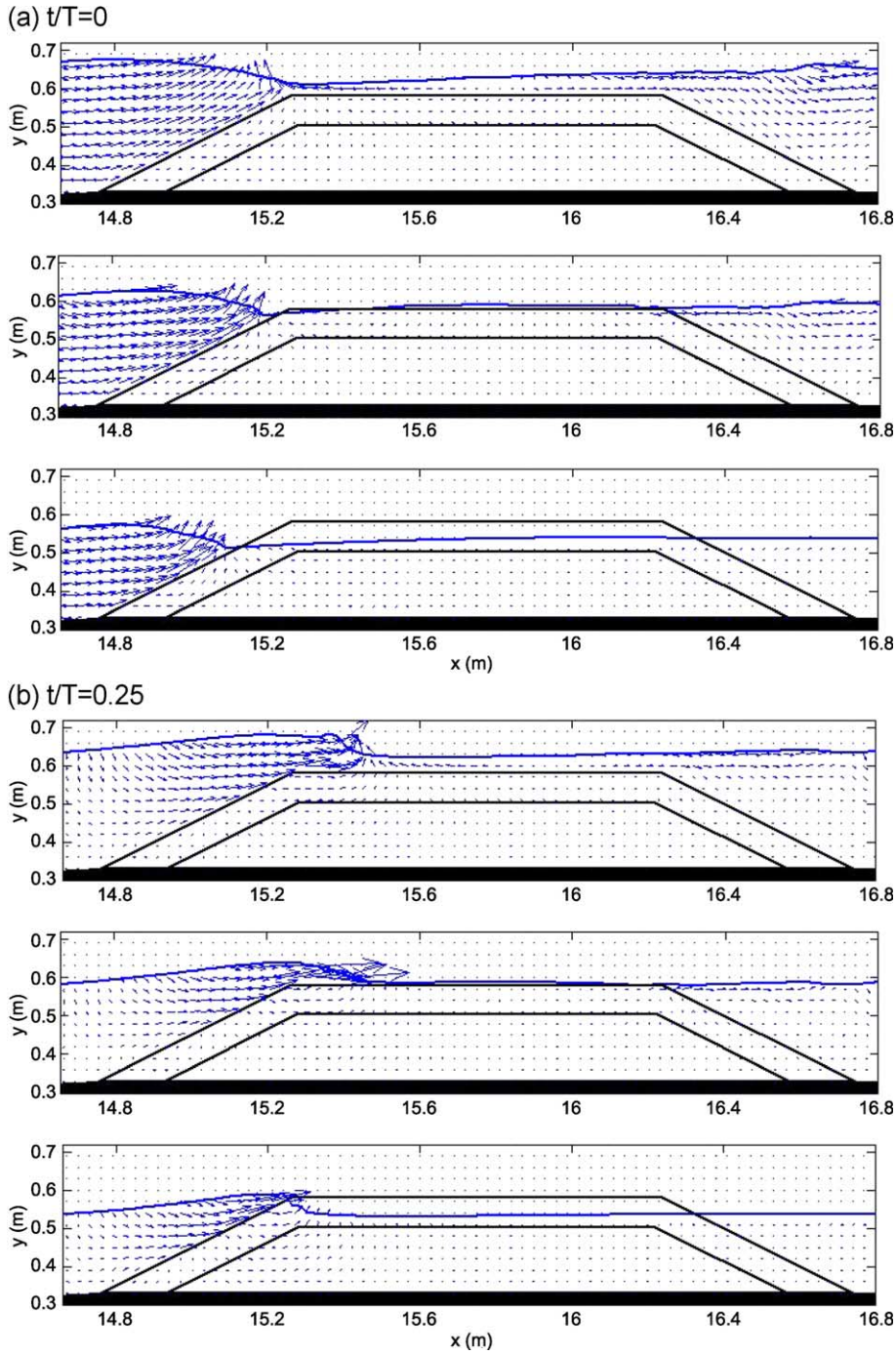

Fig. 20. Snapshots of velocity field. (a) t/T=0.0, (b) t/T=0.25, (c) t/T=0.55, (d) t/T=0.7.

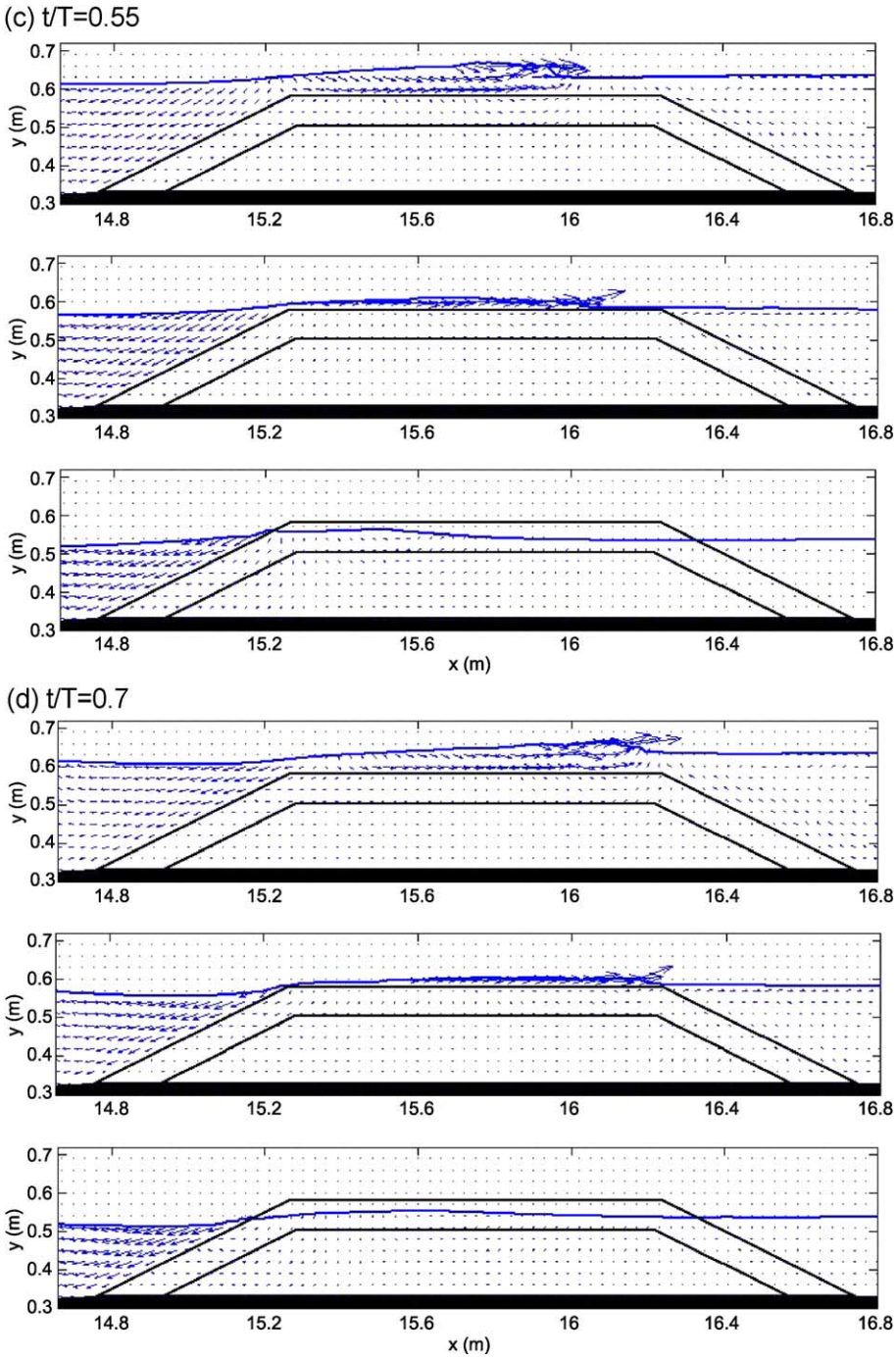

Fig. 20 (*continued*).

edge of the crest seems then to be the most vulnerable zone of the structure. When the structure is submerged, the peak velocities associated with the propagation of the roller are distributed all along the crest zone and also affect the upper part of the leeward slope.

It is important to outline the model ability to simulate the flow motions over the crest when the crown elevation coincides with the still water level. Note that the seaward edge of the crest remains alternatively emerged (t/T=0) and submerged.

In the case of the F>0 structure, as commented earlier, incident waves break over the front side slope and no overtopping occurs. As the tested structure is a rubble mound, the up-rushing wave tongue that would form over the crest if the breakwater were impermeable is transmitted into the porous media and there is finally no volume of water overtopping into the leeside water body. The portion of incident wave energy that is transmitted by the emerged rubble-mound breakwater corresponds exclusively to flow through the porous media and is thus very low. The dominant mode of energy dissipation in this case is the resistance to the flow inside the porous medium. The propagation of the dissipated wave can be clearly observed in the crest armour layer at t/T=0.55 and t/T=0.7. The oscillation is totally damped at t/T=0.

The model is then found to provide valuable information on the near-structure flow conditions. This is also true in terms of mean flow, as illustrated by Figs. 21 and 22.

The perturbation of the mean flow pattern associated with wave breaking clearly appears in these figures. The high velocities over the crest in the case of the F=0 structure, as commented above, give rise to a strong mean current over the structure crest and a vortex cell at the lee, as for the

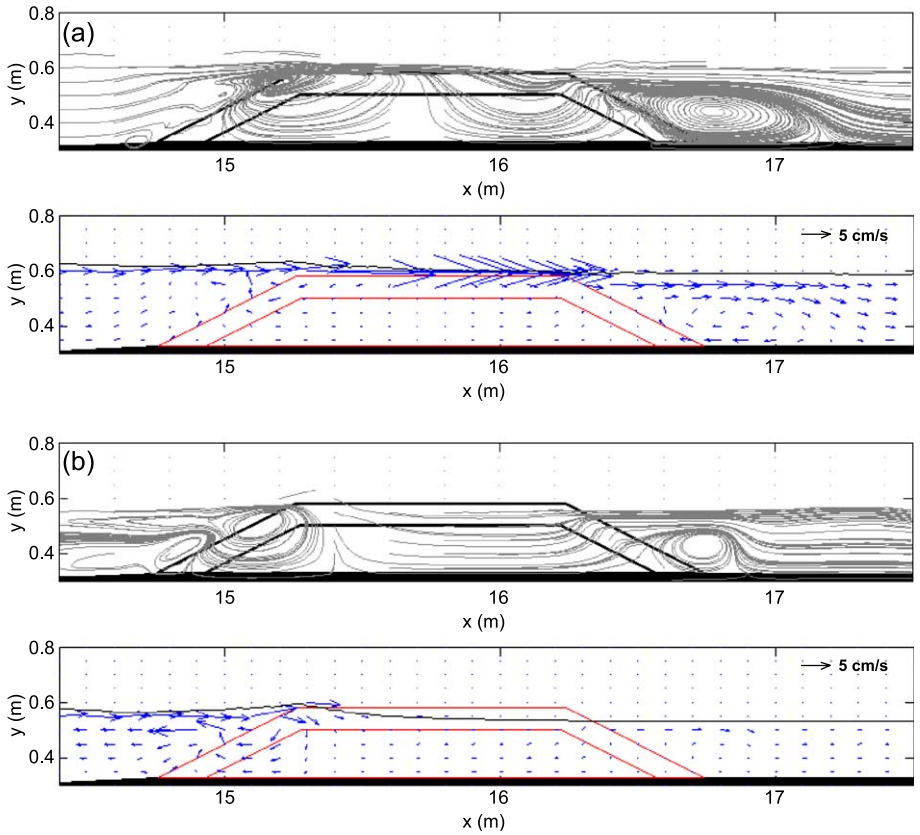

Fig. 21. Computed mean (ensemble averaged) flow. Structured freeboard (a) F=0 cm, (b) F=5 cm.

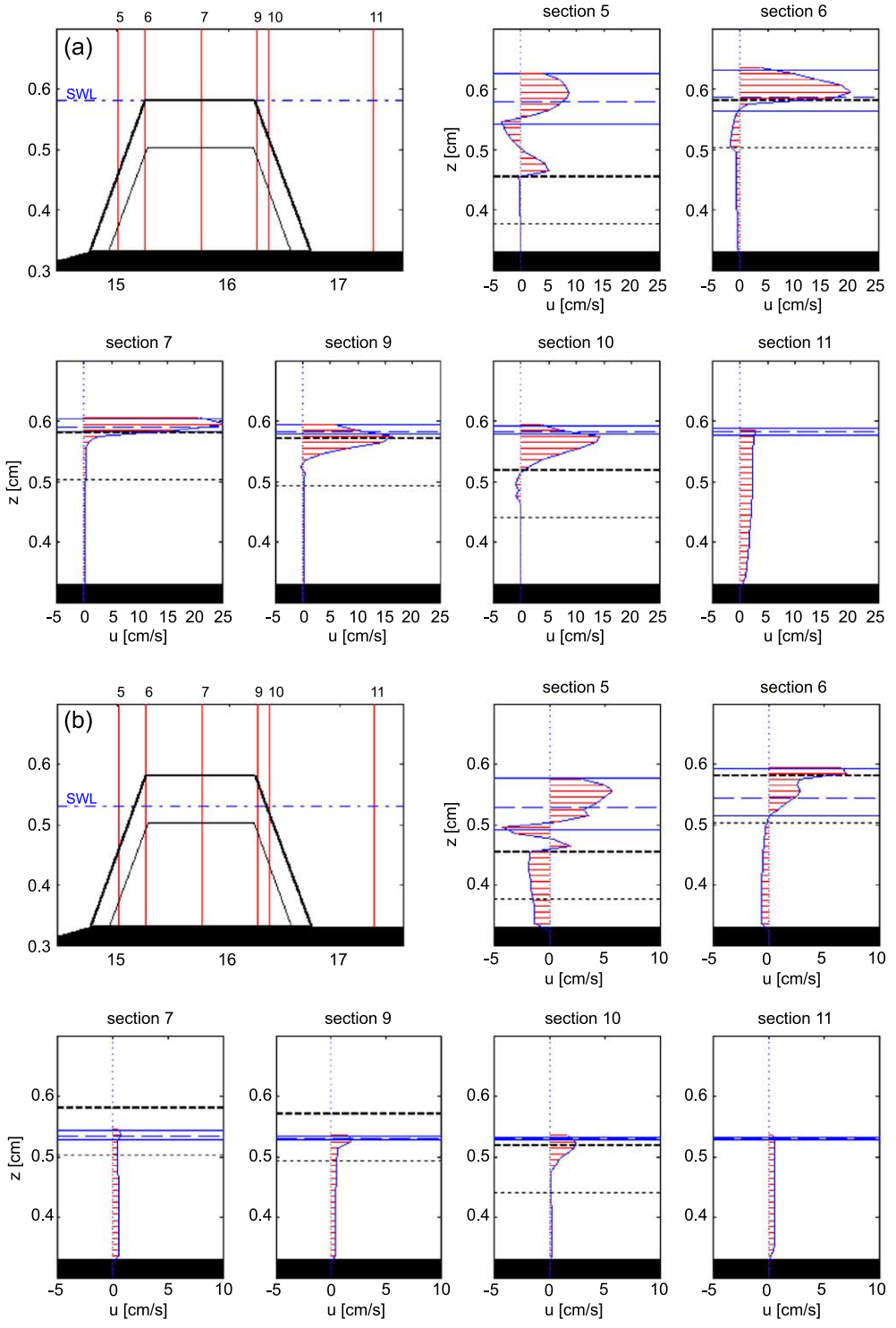

Fig. 22. Computed mean (ensemble averaged) velocity profiles. Structured freeboard (a) F=0 cm, (b) F=5 cm.

submerged structure. It is interesting to note the vertical symmetry of the stream lines pattern inside the structure. A smaller vortex cell forms at the seaward edge of the crest and confirms the vulnerability of this zone when F=0. Finally, a vortex cell of reduced dimensions appears at the seaward toe of the structure and may be responsible for scour phenomenon.

When the structure is emerged, the mean flow pattern is very different. A vortex is formed leeward, but its dimensions are reduced with respect to the other tested depths. This cell is not associated with overtopping but with transmission through the structure. On the seaward slope the mean flow shows a rather complex structure, governed by the breaking conditions. Wave surging on the slope allows a greater penetration of the flow inside the porous media, and higher velocities are observed in the armour layer and the core of the seaward part of the structure. A mean current is formed in the offshore direction. In the transmission zone the onshore mean current is considerably reduced in comparison with the previous tested water depths. Even if some of these features are similar to those described for emerged vertical porous structures by Losada et al. (1998) using second order potential flow theory, the present model is able to show the effects of the structure slope and of wave breaking on the mean flows, substantially improving previous existing works.

The spatial evolution of the mean flow pattern along the flume is more apparent in Fig. 22, which shows the vertical distribution of the ensemble-averaged velocities at different sections of the flume. In both F=0 and F=5 cm configurations, the vortices give rise to an inversion of the mean flow in the water column at Sections 5 and 6 corresponding to the seaward slope. At Section 5 the profile is rather complex, with a shoreward component above the trough level, a seaward component below and a shoreward component at the interface with the structure. As commented above, when the structure is emerged, higher velocities are reached inside the porous media and a significant mean current directed offshore can be observed in the armour layer at Section 5. This mean current is reduced at Section 6. The mean flow profile is more uniform at the other sections. The reduction of the mean current in the transmission zone with the reduction of the structure freeboard can be clearly observed at Section 11.

5. Conclusions

In this paper, the physical processes associated with near-field flow–structure interaction are investigated using a numerical model based on volume-averaging of RANS equations and corresponding k–ε equations.

A series of 2DV laboratory experiments were performed in order to calibrate and validate the model. The tested structure is a porous two-layer low-crested breakwater. Different wave conditions and water depths are considered. Submerged, zero freeboard and emerged breakwaters are tested. A flow recirculation system is included to prevent non-realistic set-up leeward of the structure.

The model is proven to reproduce with a high degree of agreement the free surface displacement in the vicinity of the structure, the pressure field inside the rubble and the velocities on the seaward slope. The shoaling and breaking effects in the seaward and crest zones, as well as the higher harmonics generation phenomenon in the transmission zone, are well simulated, whether the structure freeboard is positive, zero or negative. The present results show that this model represents a substantial improvement in the numerical modelling of LCS since it includes many processes neglected by previously existing models. Furthermore, most of the existing models based on potential theory and vertically integrated equations are able to accurately predict the free surface evolution, including breaking, but fail to give a good description of the velocity fields.

The flow recirculation system is found to deeply influence the wave height envelope patterns, the breaking conditions and the mean velocity field. The no-recirculation test simulation shows a net transport directed seaward, with very low values of the mean velocities in the transmission zone. In the recirculation case, a strong shoreward flow including a vortex cell at the lee of the structure is observed.

The influence of the structure freeboard on the near-field flow is also studied. Comparison of free surface time series along the flume and results of harmonics amplitude evolution illustrate the drastic reduction of the wave height. Numerical breaking

and mean flow patterns are presented. The model capacity in reproducing the flow conditions at a structure with a crown elevation at the still water level is outlined.

The model is proven to be a powerful tool in examining the near-field flow characteristics around low-crested structures. The data provided by the model are proven to be valid and thus can be used as an extension of the experimental database. Numerical information can be used to study physical magnitudes difficult or impossible to measure in the laboratory, such as particle velocity above the structure crest in wave breaking conditions or flow inside the porous media.

The numerical modelling based on RANS or Large Eddy Simulation (LES) is a breakthrough in our future way of approaching coastal structures design and it is currently in a relative early but solid stage. Additional work is still to be done in order to carry out a reliable use of these models for engineering design.

Additional work is being carried out to investigate the capability of the model to model random waves interaction with LCS. At present, the model includes the possibility to generate irregular waves, based on Lin and Liu (1999), as the superposition of a finite number of wave modes. Modifications of the initial code in order to include wave spectra generation and transformation has been completed and an extensive validation and calibration programme based on experimental test cases is in progress.

Furthermore, in order to analyse possible scale effects, large-scale laboratory experiments on LCS are being numerically simulated. Results on random wave interaction with LCS and scale effects will be reported elsewhere.

In the near future, this kind of modelling will become a fundamental tool in the design of coastal structures.

Acknowledgements

This study was performed within the framework of the European Union project EVK3-CT-2000-41, “Environmental DEsign of LOw-crested coastal defence Structures (DELOS)”.

Dr. Pedro Lomonaco is gratefully acknowledged for his suggestions and advice throughout the elaboration of the present paper.

References

Beji, S., Battjes, J.A., 1993. Experimental investigation of nonlinear wave propagation over a bar. Coastal Engineering 19, 151–162.

Beji, S., Battjes, J.A., 1994. Numerical simulation of nonlinear wave propagation over a bar. Coastal Engineering 23, 1–16.

Burcharth, H.F., Andersen, O.H., 1995. On the one-dimensional steady and unsteady porous flow equations. Coastal Engineering 24, 233–257.

Chorin, A.J., 1968. Numerical solution of the Navier–Stokes equations. Mathematics of Computation 22, 745–762.

D’Angremond, K., van der Meer, J.W., De Jong, R.J., 1996. Wave transmission at low-crested structures. Proc. 25th Int. Coastal Eng. Conf. ASCE, Reston, VA, pp. 2418–2427.

Dalrymple, R.A., Losada, M.A., Martín, P.A., 1991. Reflection and transmission from porous structures under oblique wave attack. Journal of Fluid Mechanics 224, 625–644.

Dattatri, J., Raman, H., Jothi Shankar, N., 1978. Performance characteristics of submerged breakwaters. Proc. 16th Int. Coastal Eng. Conf. ASCE, Reston, VA, pp. 2153–2171.

Davies, B.L., Kriebel, D.L., 1992. Model testing of wave transmission past low-crested breakwaters. Proc. 23rd Int. Coastal Eng. Conf. ASCE, Reston, VA, pp. 1115–1128.

Dick, T.M., Brebner, A., 1968. Solid and permeable breakwaters. Proc. 11th Int. Coastal Eng. Conf. ASCE, Reston, VA, pp. 2153–2171.

Diskin, M.H., Vajda, M.L., Amir, I., 1970. Piling-up behind low and submerged permeable breakwaters. Journal of the Waterways. Harbors and Coastal Engineering Division 96, 359–372.

Driscoll, A.M., Dalrymple, R.A., Grilli, S.T., 1993. Harmonic generation and transmission past a submerged rectangular obstacle. Proc. 23rd Int. Coastal Eng. Conf. ASCE, Reston, VA, pp. 1142–1160.

Gu, Z.G., Wang, H., 1992. Numerical modelling of wave energy dissipation within porous submerged breakwaters of irregular cross cross section. 23rd Int. Coastal Eng. Conf. ASCE, Reston, VA, pp. 1189–1202.

Hattori, M., Sakai, H., 1994. Wave breaking over permeable submerged breakwaters. Proc. 24th Int. Coastal Eng. Conf. ASCE, Reston, VA, pp. 1101–1114.

Hirt, C.W., Nichols, B.D., 1981. Volume of Fluid (VOF) method for dynamics of free boundaries. Journal of Computational Physics 39, 201–225.

Hsu, T.-J., Sakakiyama, T., Liu, P.L.-F., 2002. A numerical model for wave motions and turbulence flows in front of a composite breakwater. Coastal Engineering 46, 25–50.

Hur, D.-S., Mizutani, N., 2003. Numerical estimation of wave forces acting on a three-dimensional body on submerged breakwater. Coastal Engineering 47, 329–345.

Israeli, M., Orszag, S.A., 1981. Approximation of radiation boundary conditions. Journal of Computational Physics 41, 115–131.

Iwata, K., Kawasaki, K., Kim, D.S., 1996. Breaking limit, breaking and post-breaking wave deformation due to submerged structures. Proc. 25th Int. Coastal Eng. Conf., pp. 2338–2351.

Kobayashi, N., Wurjanto, A., 1989. Wave transmission over submerged breakwaters. Journal of Waterways Port, Coastal and Ocean Engineering 115, 662–680.

Kothe, D.B., Mjolness, R.C., Torrey, M.D., 1991. RIPPLE: A Computer Program for Incompressible Flows with Free Surface. Los Alamos National Laboratory. LA-12007-MS.

Lara, J.L., 2002. Análisis experimental y numérico de los procesos asociados a la rotura sobre lechos permeables. PhD thesis, University of Cantabria.

Lara, J.L., Losada, I.J., Liu, P.L., 2003. Breaking waves on a gravel slope. Part 1: Time averaged characteristics. Journal of Fluid Mechanics. Submitted for publication.

Lin, P., 1998. Numerical modeling of breaking waves. PhD thesis. Cornell University.

Lin, P., Liu, P.L.-F., 1998. A numerical study of breaking waves in the surf zone. Journal of Fluid Mechanics 359, 239–264.

Lin, P., Liu, P.L.-F., 1999. Internal wave-maker for Navier–Stokes equations models. Journal of Waterways, Port, Coastal and Ocean Engineering 125, 207–217.

Liu, P.L.-F., Lin, P., Chang, K.A., Sakakiyama, T., 1999. Numerical modeling of wave interaction with porous structures. Journal of Waterway, Port, Coastal and Ocean Engineering 125, 322–330.

Liu, P.L.-F, Lin, P., Hsu, T., Chang, K., Losada, I.J., Vidal, C., Sakakiyama, T., 2000. A Reynolds Averaged Navier–Stokes equation model for nonlinear water wave and structure interactions. Proc. Coastal Structures '99, pp. 169–174.

Lomonaco, P., Vidal, C., Revilla, J.A., Losada, I.J., 1993. Flow and pressure distribution around rubble mound protected pipelines. Proc. 2nd International Conference on Marine Waste Water Discharges, 2002.

Losada, I.J., Dalrymple, R.A., Losada, M., 1993. Water waves on crown breakwaters. Journal of Waterways Port, Coastal and Ocean Engineering 119, 367–380.

Losada, I.J., Silva, R., Losada, M.A., 1996a. 3-D non-breaking regular wave interaction with submerged breakwaters. Coastal Engineering 28, 229–248.

Losada, I.J., Silva, R., Losada, M.A., 1996b. Interaction of non-breaking directional random waves with submerged breakwaters. Coastal Engineering 28, 249–266.

Losada, I.J., Patterson, M., Losada, M.A., 1997. Harmonic generation past a submerged porous step. Coastal Engineering 31, 281–304.

Losada, I.J., Dalrymple, M.A., Losada, M.A., 1998. Wave-induced mean flows in vertical rubble-mound structures. Coastal Engineering 31, 251–281.

Loveless, J., Debski, D., 1997. Wave transmission and set-up at detached breakwaters. Proc. Coastal Dynamics'97. ASCE, Reston, VA, pp. 674–683.

Loveless, J., Debski, D., MacLeod, A.B., 1998. Sea level set-up behind detached breakwaters. Proc. 26th Int. Coastal Eng. Conf. ASCE, Reston, VA, pp. 1665–1678.

Madsen, O.S., White, S.M., 1976. Wave transmission through trapezoidal breakwaters. Proc. 15th Int. Coastal Eng. Conf. ASCE, Reston, VA, pp. 2662–2676.

Massel, S., Butowski, P., 1980. Wind waves transmission through porous breakwater. Proc. 16th Int. Coastal Eng. Conf. ASCE, Reston, VA, pp. 333–346.

Masselink, G., 1998. Field investigation of wave propagation over a bar and the consequent generation of secondary waves. Coastal Engineering 33, 1–9.

Ohyama, T., Nadaoka, K., 1992. Modeling the transformation of nonlinear waves passing over a submerged dike. 23rd Int. Coastal Eng. Conf. ASCE, Reston, VA, pp. 526–539.

Petit, H.A.H., Bosch, P. van den, Gent, M.R.A. van, 1994a. SKYLLA: wave motion in and on coastal structures; implementation and verification of modified boundaries. conditions. Delft Hydraulics Report H1780.

Petit, H.A.H., Bosch, P. van den, Gent, M.R.A. van, 1994b. SKYLLA: wave motion in and on coastal structures; implementation of impermeable slope and overtopping-boundary conditions. Delft Hydraulics Report H1780.

Rojanakamthorn, S., Isobe, M., Watanabe, A., 1989. A mathematical model of wave transformation over a submerged breakwater. Coastal Engineering in Japan 32, 209–234.

Rojanakamthorn, S., Isobe, M., Watanabe, A., 1990. Modeling of wave transformation on submerged breakwater. Proc. 22nd Int. Coastal Eng. Conf. ASCE, Reston, VA, pp. 1060–1073.

Seabrook, S.R., Hall, K.R., 1998. Wave transmission at submerged rubblemound breakwaters. Proc. 26th Int. Coastal Eng. Conf. ASCE, Reston, VA, pp. 2000–2013.

Seelig, W.N., 1980. Two-dimensional test of wave transmission and reflection characteristics of laboratory breakwaters. Technical report No. 80-1, U.S. Army Coastal Eng. Res. Center, Fort Belvoir, VA.

Sénéchal, N., Bonneton, P., Dupuis, H., 2002. Field experiment on secondary wave generation on a barred beach and the consequent evolution of energy dissipation on the beach face. Coastal Engineering 46, 233–247.

Shih, R.W.K., 1990. Permeability characteristics of rubble materialã new formulae. Proc. 22nd Int. Coastal Eng. Conf. ASCE, Reston, VA, pp. 1499–1512.

Sollit, C.K., Cross, R.H., 1972. Wave reflection and transmission at permeable breakwaters. Technical report No. 147, R.M. Parsons Lab., Dept of Civil Eng., MIT.

Troch, P., de Rouck, J., 1998. Development of two-dimensional numerical wave flume for wave interaction with rubble mound breakwaters. 26th Int. Coastal Eng. Conf. ASCE, Reston, VA, pp. 1638–1649.

Van der Meer, J.W., Petit, H.A.H., Bosh, P., van den Klopman, G., Broekens, R.D., 1992. Numerical simulation of wave motion on and in coastal structures. 23rd Int. Coastal Eng. Conf. ASCE, Reston, VA, pp. 1772–1784.

Van Gent, M.R.A., 1994. The modelling of wave action on and in coastal structures. Coastal Engineering 22, 311–339.

Van Gent, M.R.A., 1995. Porous flow through rubble-mound material. Journal of Waterway Port, Coastal and Ocean Engineering 121, 176–181.

Van Gent, M.R.A., Tönjes, P., Petit, A., van den Bosch, P., 1994. Wave action on and in permeable structures. Proc. 24th Int. Coastal Eng. Conf. ASCE, Reston, VA, pp. 1739–1753.

Vidal, C., Lomónaco, P., Migoya, L., Archetti, R., Turchetti, M., Sorci, M., Sassi, G., 2001. Laboratory experiments on flow around and inside LCS structures. Description of tests and data base. DELOS European Project, technical report.

Wibbeler, H., Oumeraci, H., 1992. Finite element simulation of wave-induced internal flow in rubble mound structures. Proc. 23rd Int. Coastal Eng. Conf. ASCE, Reston, VA, pp. 1707–1719.